Efficient Erasure Marking Technique for Delay Reduction in DSL Systems Impaired by Impulse Noise

Yuxin Zhao

Department of Electrical and Computer Engineering

McGill University

Montreal, Canada

August 2012

A thesis submitted to McGill University in partial fulfillment of the requirements for the degree of Master of Engineering.

This thesis is dedicated to my grandparents, my parents, and my husband

ABSTRACT

Digital Subscriber Line (DSL) technologies have experienced rapid development. Protecting the DSL systems against Impulse Noise (IN) is an important issue and it has recently received considerable attention. A combination of Reed–Solomon (RS) codes and interleaving is used to mitigate the destructive effects of IN. However, it is shown that the interleaving structure introduces long delay, which is certainly undesirable in high-rate transmission systems supporting interactive applications such as Internet Protocol Television (IPTV). Different techniques have therefore been proposed to reduce the interleaving delay while still being able to effectively protect the systems from IN. In particular, Error and Erasure Decoding (EED) can be used instead of Error Decoding (ED) to improve the decoder correction capability, which in turn helps reducing the required interleaving depth and delay. To fully explore the error correction capacity of the EED, reliable erasure marking becomes essential.

This thesis proposes an erasure marking technique that fully explores the correction capacity of the EED, and correspondingly, facilitates a shorter interleaving. We first study the sources that generate impulse noise and the statistics of impulse noise in DSL systems. Analytical models for the distribution of amplitude and inter-arrival time of impulse noise are also provided. Based on the statistics of impulse noise, a squared-distance based erasure marking technique is then proposed. Furthermore, analysis of selecting proper parameters for the proposed technique is developed. Finally, the Peak Signal-to-Noise Ratio (PSNR) performance of IPTV over DSL in presence of IN is investigated with the proposed erasure marking technique employed.

RÉSUMÉ

Les technologies de Ligne d'abonné numérique (DSL) ont connu un développement rapide. La protection des systèmes de DSL contre le bruit impulsif (IN) est une question importante et elle a récemment suscité attention considérable. Normalement, une combinaison decodes RS et d'entrelacement est employée pour atténuer les effets destructifs du IN. Mais, il est établi que la structure d'entrelacement introduit des longs retards qui sont certainement indésirables dans les systèmes de transmission à haut débit qui supportent des applications interactives telles que la télévision sur IP (IPTV). Donc, il existe des techniques différentes pour réduire le retard d'entrelacement tout en étant capables de protéger efficacement les systèmes contre l'IN. En particulier, le décodage d'erreur et d'effacement (EED) peut être utilisé au lieu du décodage d'erreur (ED) afin d'améliorer la capacité de correction du décodeur, qui, à son tour, contribue à réduire la profondeur de l'entrelacement requise et les retards. Pour explorer la capacité de correction d'erreurs de l'EED, une méthode fiable pour marquer les effacements devient très essentielle.

Cette thèse propose une technique de marquage de l'effacement qui utilise pleinement la capacité de correction de l'EED, et, par conséquence, entraîne un entrelacement plus court. Nous étudions d'abord les sources qui produisent l'IN et les statistiques de l'IN dans les systèmes DSL. Des modèles analytiques sur la distribution de l'amplitude et de l'intervalle entre les arrivées de l'IN sont fournis. En se basant sur les statistiques de l'IN, nous proposons une technique de marquage des suppressions basée sur la distance carrée. De plus, une analyse de la sélection des paramètres appropriés pour la technique proposée est développée. Finalement, la performance du rapport puissance maximale instantanée sur bruit (PSNR) de l'IPTV dans les systèmes de DSL en présence de l'IN est examinée avec la technique de marquage des suppressions proposée.

ACKNOWLEDGMENTS

First of all, I would like to express my deepest appreciation to my supervisor, Professor Tho Le-Ngoc for his enthusiasm, patience, kindness and guidance throughout my graduate studies at McGill University. Professor Le-Ngoc has provided me with the most inspiring research environment and has helped me through various hard times by his rich knowledge and experiences, valuable suggestions and firm supports. Without his help, my thesis would not have been possible. I would also like to acknowledge the financial support from an NSERC IRC Grant, which has enabled me to fully concentrate on my research.

As well, I would like to give my great thanks to my lab mates at the Broadband Communications Laboratory. I will surely remember all of you. Thank you for supporting me all the time and making my stay in Montreal such a pleasure and memorable experience. Especially, I would like to thank Dr. Khuong Ho Van, who gives me his full support in my research. Many thanks to Ms. Dan Zhang and Ms. Yue Gao who make my research life more colorful and enjoyable. Also, thanks to Mr. Robert Morawski's help, I built up a solid background of my research in the first year at McGill University. Great thanks to Danny, Leonardo, Chris and Mahsa who gave me valuable inputs on this thesis.

Finally, my sincere love and gratitude are devoted to my parents and my husband, for their endless love, support and encouragement.

TABLEOF CONTENTS

LIST OF FIGURES

LIST OF TABLES

LIST OF ACRONYMS

ADSL	Asymmetric Digital Subscriber Line
AWGN	Additive While Gaussian Noise
BER	Bit Error Rate
DFT	Discrete Fourier Transform
DMT	Discrete Multi-Tone
DSL	Digital Subscriber Line
ED	Error Decoding
EED	Erasure and Error Decoding
IDFT	Inverse Discrete Fourier Transform
IN	Impulse Noise
INP	Impulse Noise Protection
IPTV	Internet Protocol Television
MSE	Mean Square Error
PEIN	Prolonged Electrical Impulse Noise
PSD	Power Spectral Density
PSNR	Peak Signal-to-Noise Ratio
QAM	Quadrature Amplitude Modulation
REIN	Repetitive Electrical Impulse Noise
RS	Reed-Solomon
SHINE	Single High Impulse Noise
SNR	Signal-to-Noise Ratio
SVC	Scalable Video Coding
VDSL	Very-high-bitrate Digital Subscriber Line

LIST OF SYMBOLS

arg	argument
A_m	m^{th}transmitted frequency-domain sample
$\hat{A}_m$	Estimated transmitted symbol
B	Number of bytes in a DMT symbol
C_m	Channel frequency response on the m^{th} subcarrier
D	Interleaving depth
E	Number of impulse noise protection in bytes
$\mathrm{E}\{\cdot\}$	Expected value operator
G	Number of impulse noise time-domain samples during one DMT symbol period
I	Interleaver block length
I_m	m^{th}frequency-domain impulse noise sample
L	Length of channel impulse response
M	QAM level
N	DFT size
N_e	Number of errors in one RS codeword before decoding
N_{era}	Number of erasures in one RS codeword after de-interleaving
N_s	Number of sample groups
N_t	Selecting threshold
N_w	Window size
$P_{\mathrm{e,m}\vert\cdot}$	Conditional symbol error probability of square QAM
P_f	Probability of false-alarm
P_g	Probability of good detection
P_m	Probability of miss-detection
$\Pr\{\cdot\}$	Probability function
$\mathrm{Q}(\cdot)$	Q function

R_m	m^{th} frequency-domain received signal
S	Number of DMT symbols per RS codeword
W_m	m^{th} frequency-domain AWGN sample
Y_m	Signal-to-noise ratio on the m^{th} sub-carrier over fading channel
Z	Shift register step size
b_m	Number of bits on m^{th} sub-carrier
d_m	Minimum distance between two adjacent QAM symbols
e	Number of erasures in one RS codeword
f	Number of errors in one RS codeword
f_s	DMT symbol rate
h	Height of video
i_u	u^{th} time-domain impulse noise sample
k	RS code information length
$\min_{\gamma}$	Minimum with respect to γ
n	RS codeword length
p	Probability that the impulse occurs
$p(\cdot)$	Probability density function
r_u	Received u^{th} time-domain sample
s_u	u^{th}transmitted time-domain sample
t	Error correction capacity for RS code
v	Number of byte errors in a RS codeword caused by noise excluding IN
w	Width of video
w_u	u^{th} time-domain AWGN sample
σ^2	One-dimensional AWGN variance
$\sigma^2_{I\|\cdot}$	Average variance of impulse noise under certain condition

σ_i^2	Variance of impulse noise
σ_w^2	Variance of AWGN
γ	Distance threshold
γ_{opt}	Optimal distance threshold

Chapter 1

Introduction

1.1 Motivation

Digital Subscriber Line (DSL) technology provides broadband digital transmission over existing telephone lines. The telephone network reaches almost every home and workplace, and most telephone lines are capable of supporting DSL without major modifications. Therefore, DSL has a large customer base and great economic advantages [1]. This leads to the popularity and increasing demand for DSL technology. However, due to the properties of the twisted pair, several factors that impair DSL performance are introduced.

One of the impairments is the frequency-selective fading in DSL environment. Figure 1.1 shows an example of frequency-selective fading channel response. This frequency-selective attenuation depends on the length of the twisted copper wires used in telephone network and also on the signal reflections generated by the bridged-taps used to branch telephone lines. To cope with frequency-selective fading, multicarrier transmission, e.g., Discrete Multi-Tone (DMT), is employed by dividing the whole frequency-selective channel into several frequency-flat narrowband sub-channels, each can accommodate one sub-carrier [2].

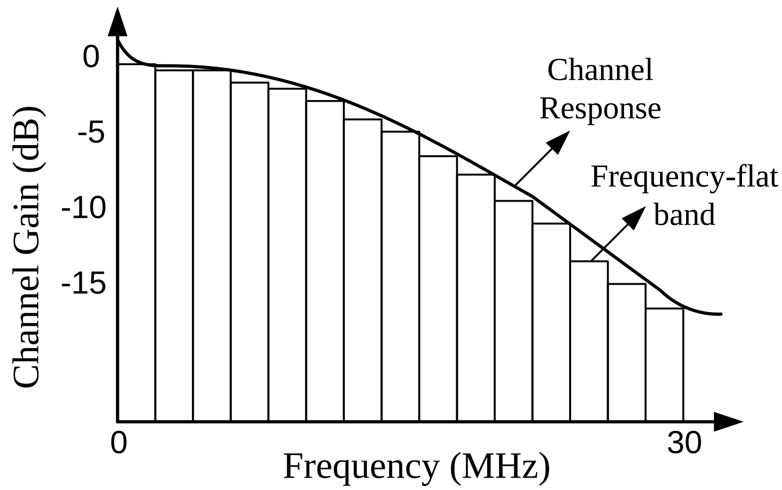

Figure 1.1 Frequency-selective fading channel response and division of frequency band into many small frequency-flat narrow band sub-channels

Another factor affecting the performance of DSL is crosstalk. Crosstalk is caused by electromagnetic coupling between different telephone lines within the same bundle. There are two kinds of crosstalk. The first one is near-end crosstalk (NEXT), which is the interference at the same end as the transmitter. The other one is far-end crosstalk (FEXT), which is the interference at another end of the transmitter as shown in Figure 1.2. The total crosstalk onto a telephone line is cumulative, since it includes the crosstalk from every other telephone line in the same bundle. This cumulative crosstalk represents a major source of interference in DSL systems.

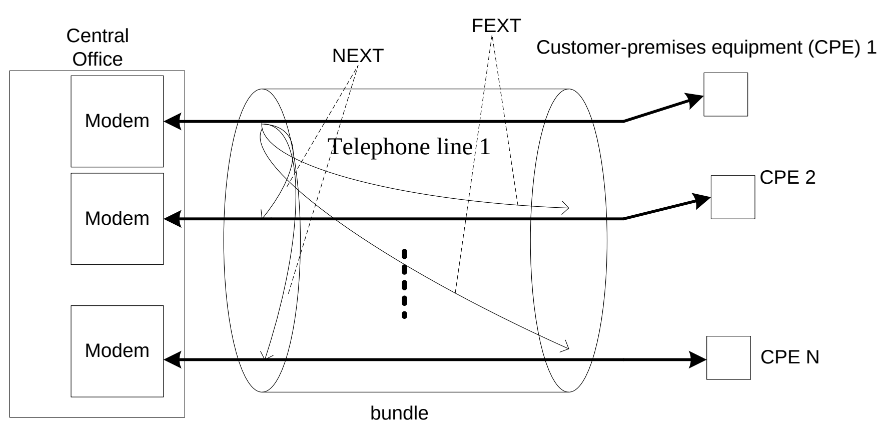

Figure 1.2 Crosstalk in DSL system

The background noise is another factor that affects DSL performance. The background noise is mainly thermal noise from the environment and is usually modeled as Additive White Gaussian Noise (AWGN). However, the effects of AWGN in current DSL system are negligible with proper designed bit-loading and certain Signal-to-Noise Ratio (SNR) margin.

In addition to the aforementioned factors, Impulse Noise (IN) is another type of noise that can severely degrade DSL performance. IN has a very high amplitude and long duration which can be up to several hundreds of microseconds. Typically, IN noise generated by a variety of sources, such as electronic equipments, switching gears, and motors in a DSL network. The power of IN is much higher than that of AWGN, and the designed SNR margin is not large enough to protect the DSL system from IN. Hence, the DSL designed to account for AWGN can no longer sustain a low BER in the presence of IN. This implies that errors will occur more frequently at the receiver. For some high data rate transmission schemes, frequent errors lead to severe packet-loss, and hence severely damaging the quality of the transmission.

In order to combat with IN in DSL systems, existing techniques involve the combination of Reed-Solomon (RS) coding and interleaving [3]. In the presence of IN, the occurrence of consecutive errors implies that the number of errors in an RS codeword may exceed the error correction capacity. Therefore, interleaving/de-interleaving is employed to spread the consecutive errors into several RS codewords and thereby limit the number of errors in each RS codeword below its error correction capacity. Although longer interleaving will spread the errors more randomly, the delay caused by interleaving/de-interleaving is not desirable. For example, some applications such as live video transmission require the delay be less than 8 ms [4]. Also, interactive applications are very sensitive to latency. One way of reducing the interleaving delay is to increase the error correction capacity of RS codes by employing error and erasure decoding (EED) instead of error decoding (ED). Since the number of errors and erasures that EED can correct is twice as many as that of ED, shorter interleaver is required to spread the erroneous RS symbols. To fully explore the error correction capacity of the EED, it is necessary to correctly mark the actual erasures while at the same time not missing any suspected erasure. The question of marking exact erasures inspires many studies on erasure marking techniques (see, e.g., [3]). Although in those studies the interleaving delay has been shortened, there is still space to further reduce the delay by marking more accurate erasures.

1.2 Research Objectives and Summary of Contributions

This thesis attempts to address the issue of accurately marking erasures to achieve better interleaving delay reduction in DSL systems impacted by impulse noise. Specifically, the following aspects have been investigated.

First, we examine the sources of impulse noise by carrying out several measurements. We characterise impulse noise generated by different appliances through modeling the distribution of amplitude and inter-arrival time.

Then, we look further into the question of accurately marking erasures in order to perform EED. As discussed before, the improvement in error correction capacity of EED will reduce the requirement for interleaving depth, and hence, the interleaving delay. Theoretically, when the error correction capacity of EED is fully explored, the corresponding interleaving delay can be reduced to half of that of ED [3]. This requires that only the erroneous symbols be marked. The author in [5] proposes a squared-distance based erasure marking technique. It first marks the individual symbols as erasure if the distance between the received symbol and the corresponding demodulated one exceeds a certain distance threshold γ. Then, the DMT symbol containing any erasure is erased. However, illustrative results in [5] show that this marking method cannot reduce the interleaving delay to half of that of ED since many erasures are falsely marked that the number of erasures in RS codewords exceeds the error correction capacity of EED. We improve the squared-distance based erasure marking technique in [5] as follows. We first mark the individual symbols as erasure using the squared-distance condition. We optimize this distance threshold by minimizing the sum of miss-detection (i.e., no erasure is marked in the presence of IN) probability P_m and false-alarm (i.e., an erasure is marked in the absence of IN) probability P_f. Then, the number of erasures in a window of size N_w is counted. If this number exceeds a selecting threshold N_t, the whole window will be erased. Also, the method of selecting proper γ and N_t for this erasure marking technique is studied.

Since currently high data rate applications such as live video transmission have a higher requirement for delay [6], we test the proposed technique with video transmission over DSL system. The interleaving delay performance and Peak Signal-to-Noise Ratio (PSNR) that measures the video quality are investigated.

1.3 Thesis Outline

The rest of this thesis is organized as follows.

Chapter 2 investigates the sources of impulse noise, followed by impulse noise modeling, taking into account the amplitude distribution, inter-arrival time distribution and power spectral density (PSD).

Chapter 3 introduces a general DSL system model. Current impulse noise protection using RS coding and convolutional interleaving will be explained.

Chapter 4 proposes a squared-distance based erasure marking technique to fully explore the error correction capacity of EED. An analytical method of selecting optimal distance threshold γ will be provided. The effects of N_t on delay reduction performance are studied to select the proper parameters for the proposed erasure marking technique. Illustrative results on interleaving delay will be presented together with some remarks.

Chapter 5 presents simulation results when the proposed erasure marking technique is applied to video transmission over DSL systems. In particular, the delay reduction performance and PSNR performance are presented.

Chapter 6 concludes the thesis and suggests some future research work.

Chapter 2

Impulse Noise in DSL Environment

In this chapter, we investigate the sources and characterization of impulse noise in DSL environment. This chapter is arranged as follows. In Section 2.1, the sources that generate impulse noise will be summarized. In Section 2.2, statistical characterization of impulse noise will be studied, and several impulse noise models will be provided. Section 2.3 summarizes this chapter.

2.1 Sources of Impulse Noise

Impulse noise is described as a kind of noise that has a strong amplitude in a short duration with unpredictable occurrence. Existing in DSL environment, impulse noise can be induced by man-made equipment, vehicles, electrical appliances, fluorescent lighting, and so on. In home environment, impulse noise can be generated by some home appliances with strong operating power, such as vacuum cleaner and hair dryer. Those appliances have motors which generate energy spikes when operating. Therefore, it is likely that these spikes induce impulse noise to the DSL telephone line [7].

2.2 Characterization of Impulse Noise

2.2.1 Impulse Noise Measurements

Measurements have been carried out to record statistics of impulse noise from different home appliances. The statistics of impulse noise consist of time domain and frequency domain statistics. In the time domain, the amplitude, duration and inter-arrival time (as shown in Figure 2.1) of impulse noise are measured. In the frequency domain, the power spectral density reflects the strength of impulse noise on different frequency bands.

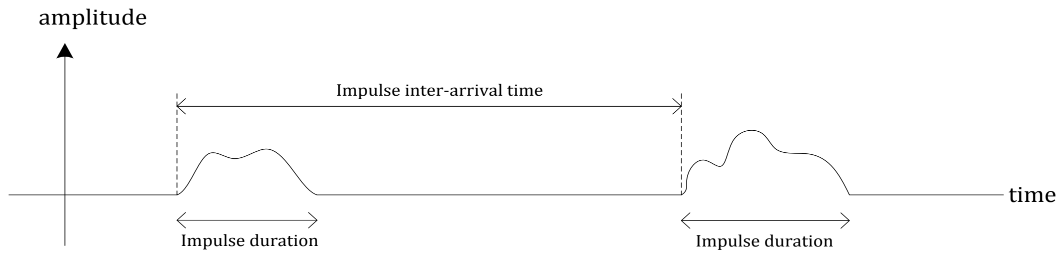

Figure 2.1 Time-domain statistics of impulse noise

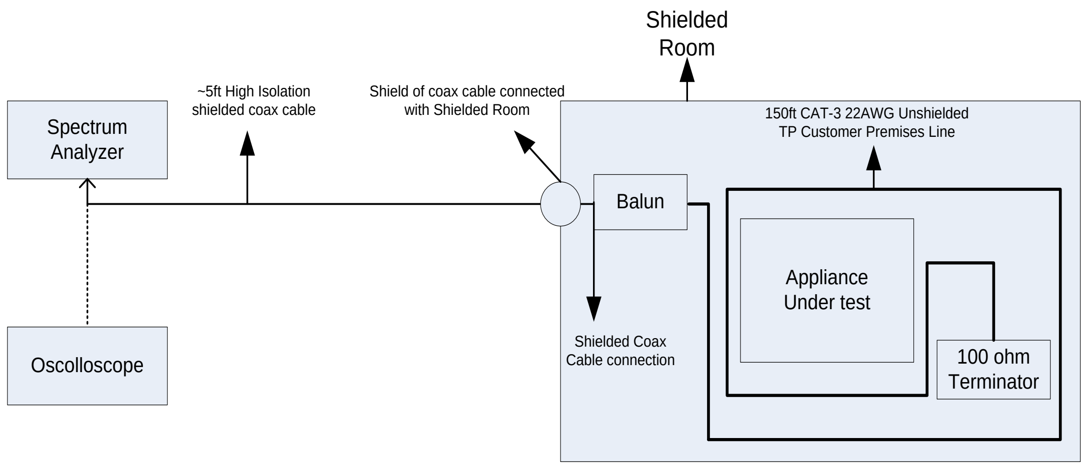

Figure 2.2 Measurement setup

The measurement is setup as depicted in Figure 2.2. The appliances under test are located in a shielded room to isolate from other interference. In particular, they are placed near the unshielded twisted wire loop. Out of the shielded room, the spectrum analyzer and oscilloscope are used to record the data regarding the IN characteristics. It is noted that since 50-to-100 Ohm Balun adapters have high attenuation below 300 kHz and Very-high-speed Digital Subscriber Line 2 (VDSL2) uses frequency up to 30 MHz, we only consider the results in the frequency bands from 300 kHz to 30 MHz.

Impulse noise is detected when both appliances are operating. The recorded time-domain waveforms for hair dryer and vacuum cleaner are shown in Figures 2.3 and 2.4 respectively.

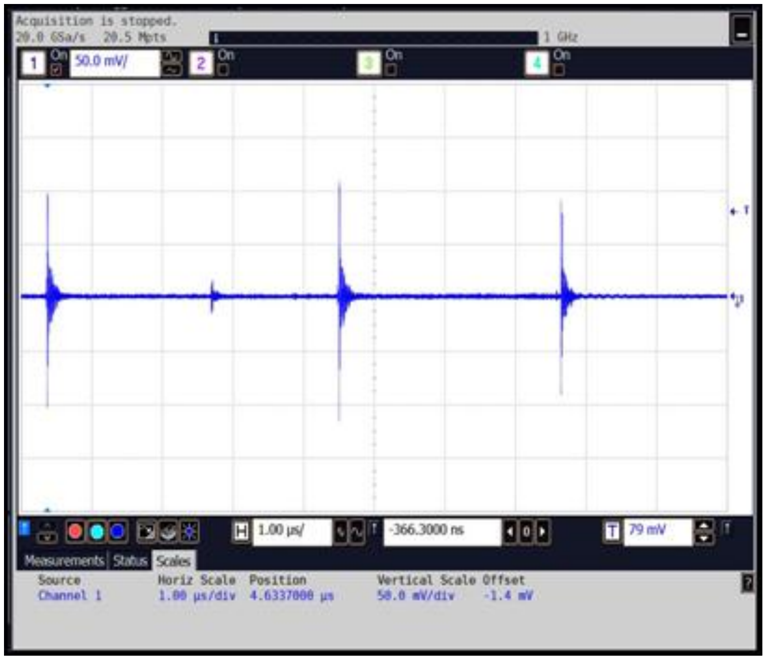

Figure 2.3 Time-domain waveform for impulse noise generated by hair dryer

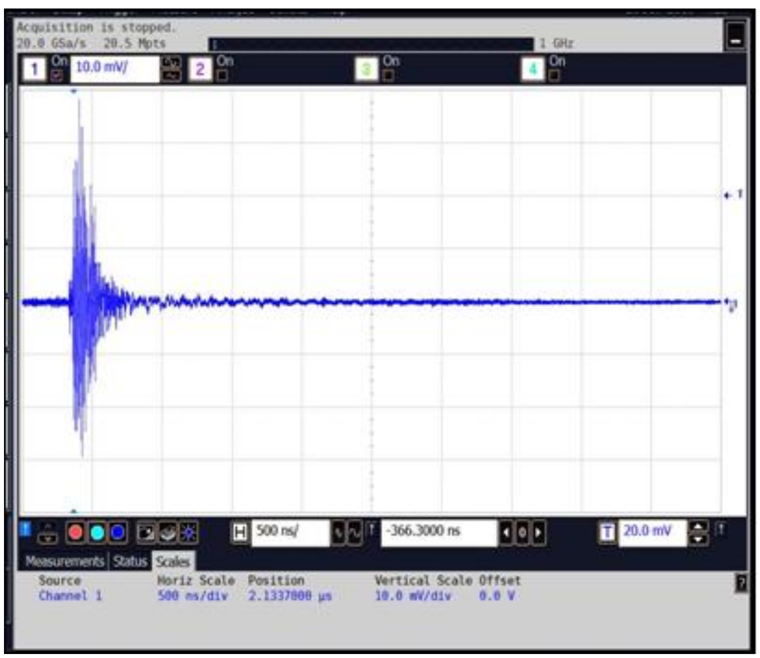

Figure 2.4 Time-domain waveform for impulse noise generated by vacuum cleaner

From Figures 2.3 and 2.4, it can be seen that the time-domain waveforms in these cases reflect the bursty nature of impulse noise. Generally, impulse noise generated by the hair dryer exhibits some repetitive behaviour, whereas it is not the case for the vacuum cleaner. In addition, in Figure 2.3, the impulse noise from the hair dryer has a short duration of 250 ns and its amplitude is between -0.12 V (Volts) and 0.12 V. On the other hand, Figure 2.4 shows an impulse of a larger duration of 500 ns whose amplitude is between -0.03 V and 0.04 V.

For amplitude data collection, the peak values of impulse sample, x, are recorded. All amplitude sample values are divided into N_s groups, each of size $\Delta x= (x_{\max}-x_{\min})/N_s$, with $x_{\min}$ and $x_{\max}$ being the minimum and maximum value, respectively. Then, the probability density $\Pr\{x_{min}+j\Delta x<x\leq x_{min}+(j+1)\Delta x\}/\Delta x$, j=0, 1,…N_s-1, is plotted in Figure 2.5.

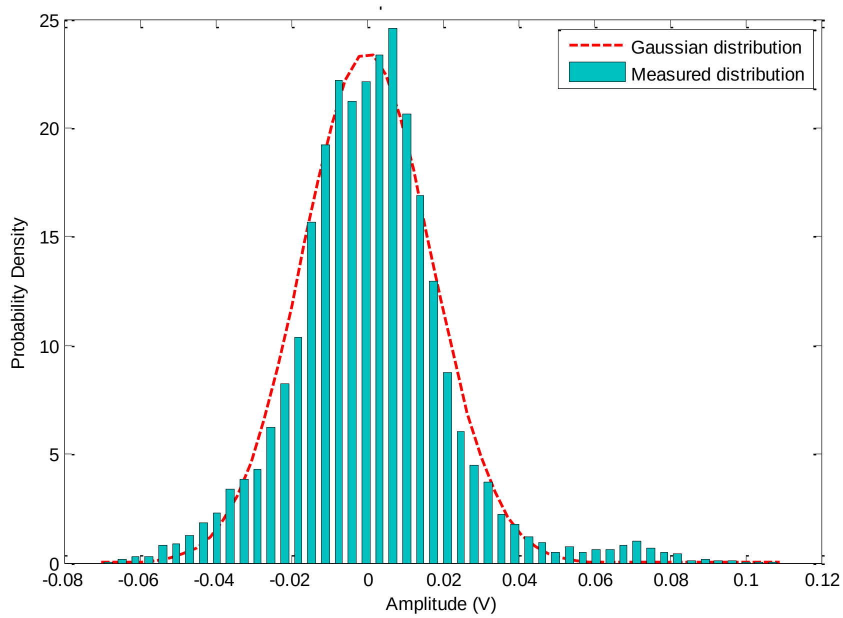

Figure 2.5 Amplitude distribution for impulse noise generated by hair dryer

It is clear from Figure 2.5 that the measured amplitude distribution is quite symmetric about 0 V and closely follows the Gaussian distribution with the following probability density function (shown by the dashed curve):

$$p(x)=\frac{1}{\mu_0\sqrt{2\pi}}\mathrm{e}^{-\frac{x^2}{2\mu_0{}^2}} \tag{2.1}$$

where the standard deviation μ_0=0.017 V.

We also measured the inter-arrival time, t, between two adjacent impulses. All sample values are divided into N_s groups, each of size $\Delta t= (t_{\max}-t_{\min})/N_s$, with $t_{\min}$ and $t_{\max}$ being the minimum and maximum value, respectively. Then, the probability density $\Pr\{t_{min}+j\Delta t<t\leq t_{min}+(j+1)\Delta t\}/\Delta t$, j=0, 1,…, (N_s-1), is calculated for different intervals, as plotted in Figure 2.6.

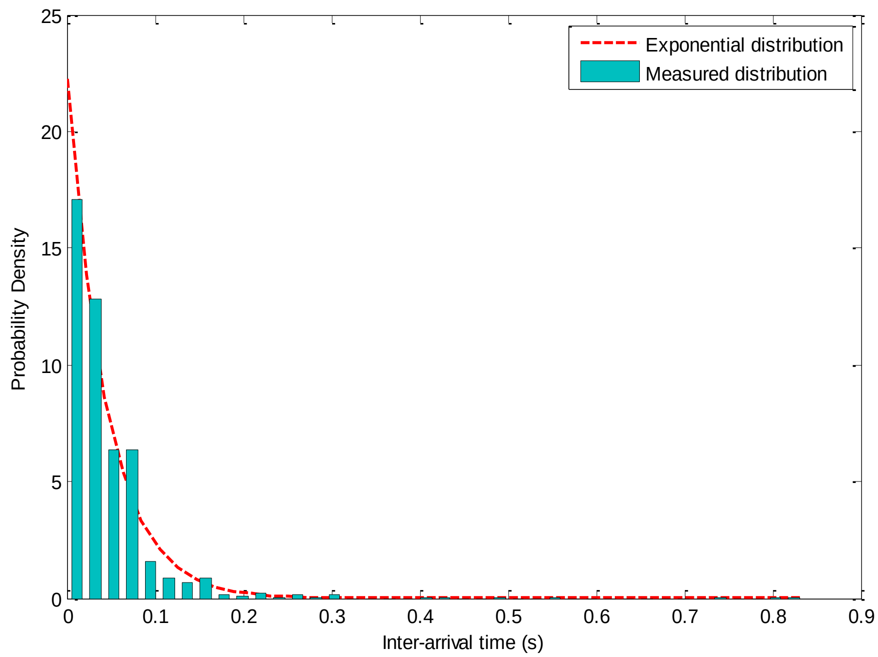

Figure 2.6 Inter-arrival time distribution for impulse noise generated by hair dryer

From Figure 2.6, it is clear that the inter-arrival time mainly concentrates on 20-100 ms (milliseconds). As well, the number of inter-arrival samples decreases significantly for inter-arrival time larger than 100 ms. The measured inter-arrival time distribution follows an exponential function:

$$p(t) = \lambda e^{-\lambda t}, \qquad t \geq 0 \tag{2.2}$$

where λ =22.71 Hz (i.e., the average inter-arrival time is$1/\lambda$=40ms).

In other words, from the measured results, impulse noise generated by hair dryer can be represented by a Bernoulli-Gaussian process, i.e., a product of a Bernoulli process and a Gaussian process as follows [8]:

$$i_u = b_u g_u, \tag{2.3}$$

where b_u is the Bernoulli process, i.e., an i.i.d. sequence of b_u=1 with probability of p=1/ λ [9] and b_u=0 with probability of (1-p); and g_u is a Gaussian noise with zero mean and variance μ_0^2 .

Impulse noise generated by vacuum cleaner is also investigated. The measured results plotted in Figure 2.7 indicate that the distribution of inter-arrival time mainly concentrates on the area less than 100 ms and it follows an exponential distribution (dashed line in Figure 2.7), but with λ =14.99 Hz.

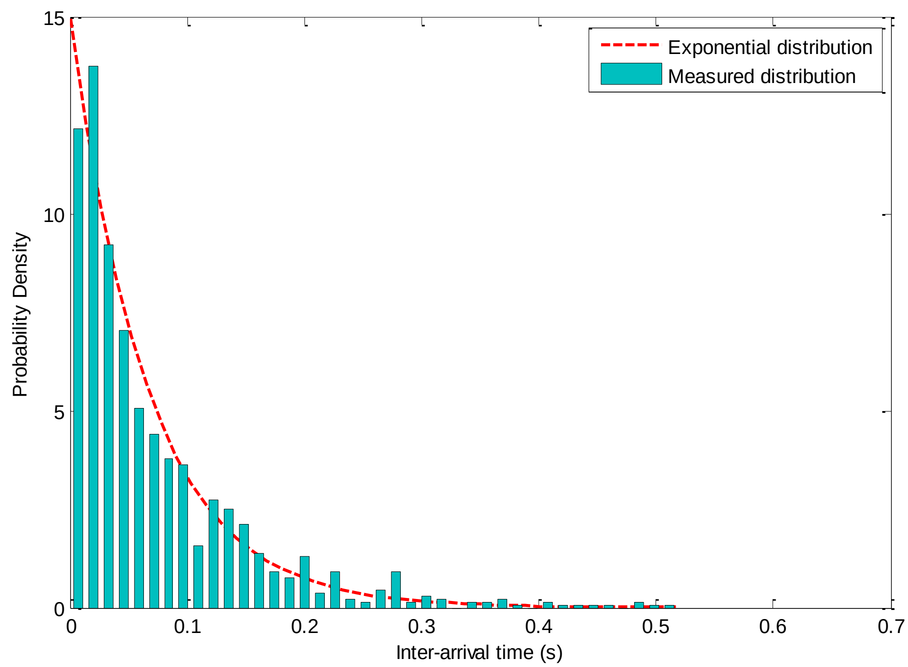

Figure 2.7 Inter-arrival time distribution for impulse noise generated by vacuum cleaner

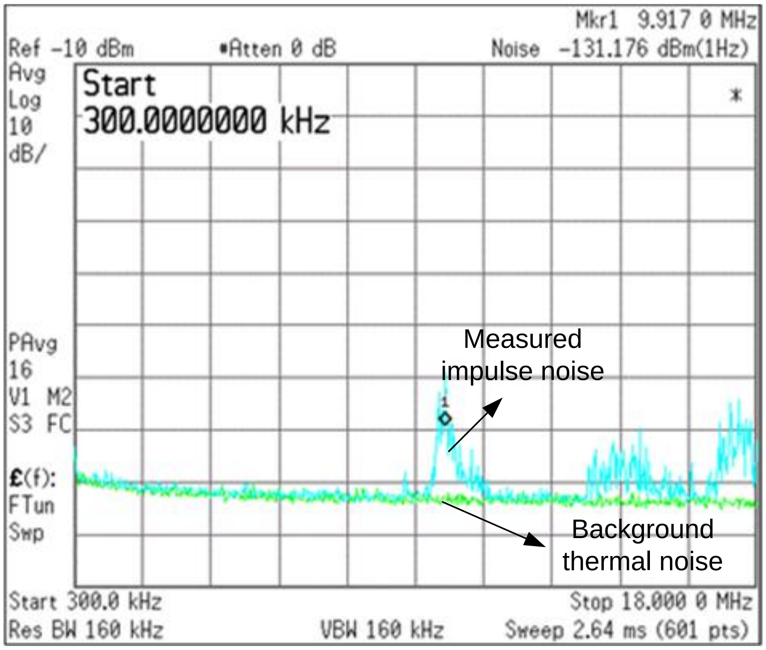

Figure 2.8 Power spectral density for impulse noise generated by hair dryer

The measured power spectral density shown in Figure 2.8 indicates that the hair dryer generates noise with the highest power level of -131 dBm/Hz (i.e., 10 dB higher than background thermal noise) around 9.9 MHz and 17 MHz with a bandwidth of 900 kHz.

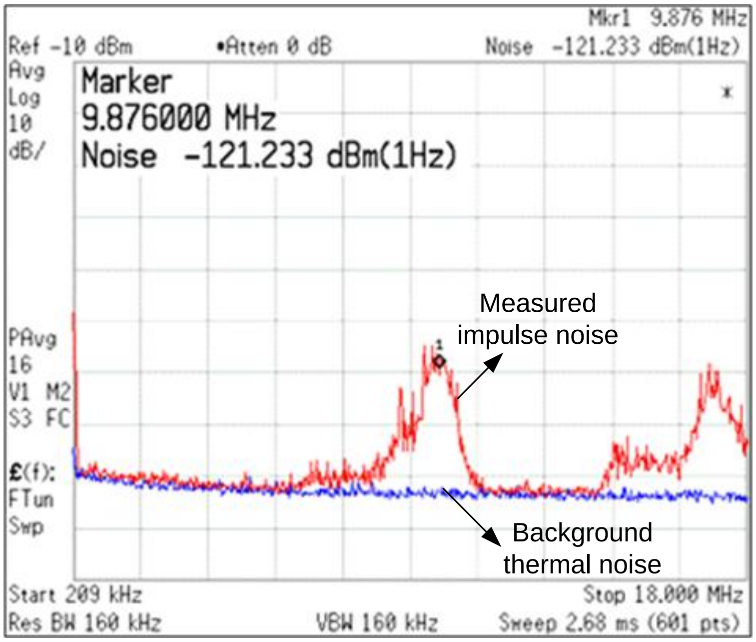

Figure 2.9 Power spectral density for impulse noise generated by vacuum cleaner

Figure 2.9 shows that the vacuum cleaner generates impulse noise with the level of approximately -121 dBm/Hz (i.e., 20 dB stronger than the background thermal noise) around 9.9 MHz and 17 MHz (identical to those of the hair dryer) with a bandwidth of approximately 900 kHz each.

As can be seen the power level of IN is much higher than the background thermal noise, and it may occupy a wide frequency band.

2.2.2 Impulse Noise Models

To facilitate the analysis and practical tests of the effects of impulse noise on DSL system performance, several impulse noise models have been proposed. Bernoulli-Gaussian process, which is consistent with our measured results, has been widely used to model impulse noise in analysis, e.g., in [8]. For DSL practical performance testing and verification, various standardized IN models have been suggested in [10]. The model suggested for North America is the repetitive electrical impulse noise (REIN), a product of repetitive pulse cycles and a Gaussian process represented by:

$$i_u = f_u g_u \tag{2.5}$$

where f_u is a repetitive pulse and g_u is a Gaussian process. In [10], the suggested REIN model has duration of 100 μs, and a pulse repetition rate of 120 Hz.The PSD of REIN is given as:

$$PSD_{REIN}(f) = \begin{cases} -\dfrac{116\text{dBm}}{\text{Hz}}, & \text{for } f < 2.2 \text{ MHz} \\ \dfrac{max\left\{-116 - 40\, log_{10}\left(\frac{f}{2.2\times 10^6}\right), -150\right\} \text{dBm}}{\text{Hz}}, & \text{for} f \geq 2.2 \text{ MHz} \end{cases} \tag{2.6}$$

It can be seen from the PSD model that REIN concentrates on the frequency band below 2.2 MHz and the power decreases with a slope beyond 2.2 MHz. In this thesis, we will use REIN for some simulations. Another model suggested in [10] is the single high impulse noise (SHINE) model, a single Gaussian impulsion with duration larger than 10 ms and PSD of -86 dBm/Hz. In addition, prolonged electrical impulse noise

(PEIN), is also suggested with varying duration (e.g., 1.2, 2.4 and 3.6 ms with probability 0.647, 0.229, and 0.124, respectively). The inter-arrival time of PEIN, between 4 seconds to 1094 seconds, follows the distribution $p(t) = 1/(t\ln(273.5))$. Reference [11] provides analytical modeling of IN including time-domain characteristics and PSD. In [11], the amplitude probability density is approximated by a Weibull distribution, and inter-arrival time follows an exponential distribution which is consistent with our measured results.

2.3 Chapter Summary

In this chapter, we first provided the definition of impulse noise. The sources that generate impulse noise have also been discussed. Based on the measurements of impulse noise carried out with different home appliances, we provided analytical models for both amplitude and inter-arrival time distributions. Also, the PSD of measured impulse noise is presented. Finally, some suggested impulse noise models are provided.

From all the measurements and analysis, we conclude that impulse noise generated by hair dryer follows a Bernoulli-Gaussian process. Thus, in the following chapters, we will use Bernoulli-Gaussian impulse noise model for most simulations and analysis. The REIN model will be used in some simulations since this is a model suggested for North America DSL system performance tests.

Chapter 3

DSL System Overview

In this chapter, we introduce the overall DSL system model and address the issue of reducing interleaving delay by using EED. This chapter is organized as follows. In Section 3.1, an introduction of DSL environment will be provided with a general system model. The impulse noise protection scheme using RS coding and interleaving will be discussed. Section 3.2 will explain the error and erasure decoding and discuss several erasure marking techniques. Finally, Section 3.3 concludes this chapter.

3.1 Introduction of DSL System

3.1.1 General DSL System Model

Figure 3.1 shows the block diagram of a general DSL system. Input data is first grouped into segments of k bytes to encoded into (n, k) RS codewords defined over the Galois field GF(2^8). The codeword is then interleaved. Next, coded information is passed through the DMT transmitter to form DMT symbols.

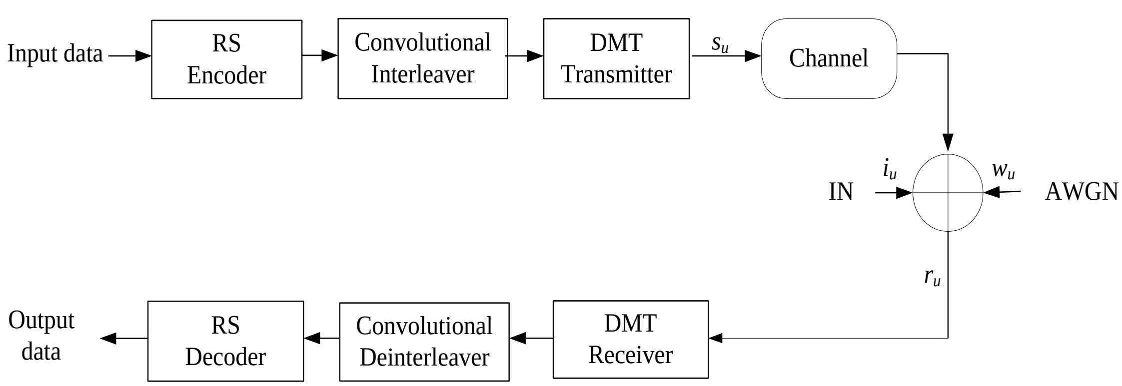

Figure 3.1 DSL system model

Figure 3.2 shows a diagram of DMT transmitter. First, bit-loading assigns different number of bits to different sub-carriers. The number of bits on m^{th} sub-carrier is calculated as [2]:

$$b_m = \log_2(1 + \frac{Y_m}{\Gamma}) \qquad (3.1)$$

where Y_m is the signal-to-noise ratio on the m^{th} sub-subcarrier:

$$Y_m = |C_m|^2 E\{|A_m|^2\}/\sigma_w^2.$$

C_m is the channel frequency response, $E\{|A_m|^2\}$ is the average transmitter signal power, and σ_w^2 is the variance of AWGN. Γ=9.8$-\Gamma_c + \Gamma_m$ in dB, is the SNR gap which defines the gap from the theoretical Shannon limit assuming a target bit error rate (BER) of 10^{-7}[2]. Γ_c is the coding gain, which is zero in this thesis as *uncoded* *M*-QAM is assumed, and Γ_m is the SNR margin. When Γ_c and Γ_m are zero, Γ is 9.8 dB to load b_m bits for *M*-QAM scheme to achieve a target BER of 10^{-7}, where b_m=$\log_2 M$ [2]. SNR margin of 6dB or 9 dB is added to protect DSL systems against signal or noise power fluctuation. Correspondingly, in a normal transmission situation, with the set SNR margin of 6 dB or 9 dB, a BER of less than 10^{-22} can be obtained [10], which indicates the effect of AWGN is negligible. However, in the presence of IN, it has a much higher power than that of AWGN (e.g., 24 dB higher in DSL standard [10]). Then, the 6dB or 9dB SNR margin is not high enough to protect the system from IN and this will increase the BER to higher than 10^{-7}. Therefore, without other protection technique, DSL system performance cannot be maintained in the presence of IN.

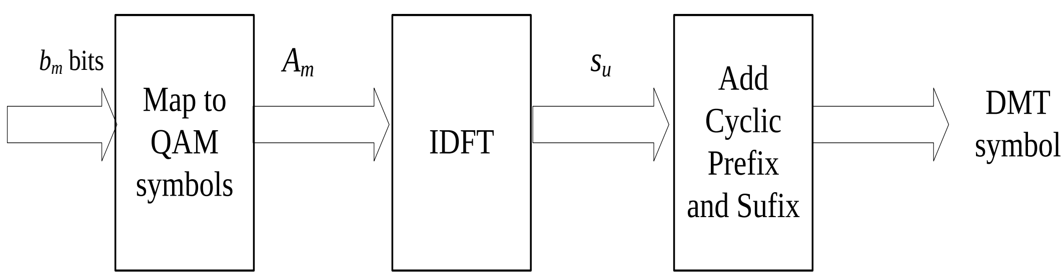

Figure 3.2 DMT transmitter

The input data is mapped to QAM symbols A_m. Let M_m denote the constellation size on m^{th} sub-carrier and $M_m = 2^{b_m}$. Each block of N QAM symbols is then converted into time-domain samples s_u, $u = 0, 1, \ldots, N-1$, using Inverse Discrete Fourier Transform (IDFT),

$$s_u = \frac{1}{\sqrt{N}} \sum_{m=0}^{N-1} A_m e^{\frac{j2\pi mu}{N}}, \tag{3.2}$$

where N is the IDFT size. Then, cyclic prefix and suffix are added to prevent Inter-Symbol Interference (ISI) and the complete DMT *symbol* is formed.

DMT symbols are passed through the channel and corrupted by both AWGN and IN. The u^{th} time-domain sample is given as

$$r_u = (\mathbf{c} * \mathbf{s})_u + w_u + i_u, \tag{3.3}$$

where $\boldsymbol{c} = \{c_0, c_1, \ldots, c_L - 1\}$ is the channel impulse response with length L, $\mathbf{s} = \{s_0, s_1, \ldots, s_{N-1}\}$, * denotes the convolution operator, w_u is the time-domain AWGN sample with zero mean and variance of σ_w^2, and i_u presents the time-domain IN sample. Figure 3.3 shows a DMT receiver. The received time-domain samples in each DMT symbol are converted back to frequency domain samples by discrete Fourier transform (DFT)

$$R_m = \frac{1}{\sqrt{N}} \sum_{u=0}^{N-1} r_u e^{-j2\pi mu/N} = C_m A_m + I_m + W_m, \tag{3.4}$$

where $m = 0, 1, \ldots, N-1$,

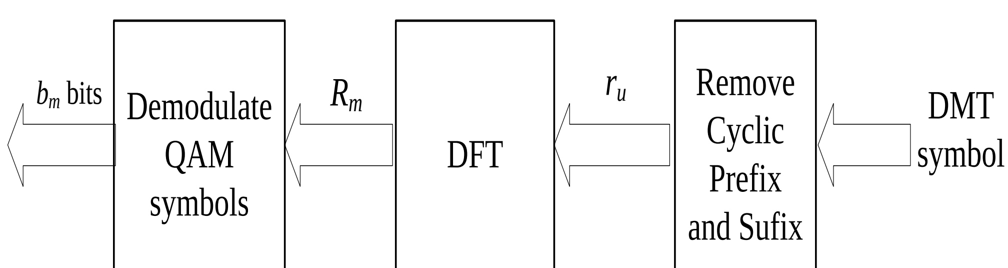

Figure 3.3 DMT receiver

and

$$I_m = \frac{1}{\sqrt{N}} \sum_{u=0}^{N-1} i_u e^{-j2\pi mu/N} \tag{3.5}$$

$$W_m = \frac{1}{\sqrt{N}} \sum_{u=0}^{N-1} w_u e^{-j2\pi mu/N} \tag{3.6}$$

From (3.4) and (3.5), even if one time-domain IN sample happens during a DMT symbol, errors on consecutive tones (error burst) may occur since the DFT distributes the high IN power over the whole DMT symbol. In such a case, it is possible that the entire DMT symbol is contaminated. As a result, the system BER can be significantly increased.

After DFT, the QAM symbol is then demodulated. Finally, the signal is de-interleaved and decoded to recover the original data.

3.1.2 Impulse Noise Protection Using RS Coding and Convolutional Interleaving

In DSL systems, RS coding and convolutional interleaving are employed to protect the system from IN distortion. RS codes are used for correcting errors in data transmission. For an (n, k) RS code defined over GF(2^8) in DSL, the decoder can correctly decode the original codeword provided that $2f+e \le n-k$, where f is the number of errors and e is the number of erasures in an RS codeword [12]. Hence, for ED (i.e., e=0), the maximum number of errors can be corrected in an RS codeword is $\lfloor (n-k)/2 \rfloor$, where $\lfloor x \rfloor$ signifies the floor operation. For EED, the maximum number of erasures can be corrected is (n-k) (i.e., f=0).

Interleaving involves rearranging the data into a non-continuous way as shown in Figure 3.4. De-interleaving does the opposite operation to get data back into the original order. When consecutive errors occur during transmission, the operation of de-interleaving can spread the errors into different codewords as illustrated in Figure 3.4.

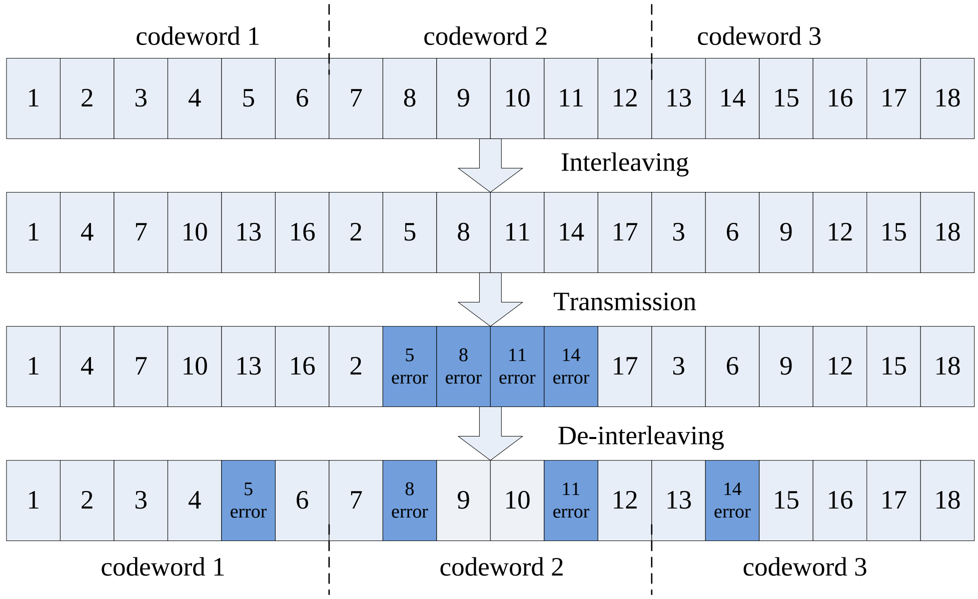

Figure 3.4 Interleaving and de-interleaving to spread consecutive errors

Since convolutional interleaving/de-interleaving achieves the same performance with half delay as compared to block interleaving/de-interleaving [13], it is usually employed in DSL systems. Figure 3.5 illustrates a typical convolutional interleaving structure in DSL systems with a block size of I bytes ($n = qI$, where q is the number of interleaver blocks per RS codeword). Each row has $(l-1)$ shift registers (where l=1,…, I is the row index) with a step size of Z bytes. At each time, a group of$I$ bytes data is fed into the shift registers, and the oldest bytes in shift registers are shifted out, becoming the output vector. Due to the delay caused by shift registers, the byte at l^{th} row is delayed by $(l-1)Z$ bytes.

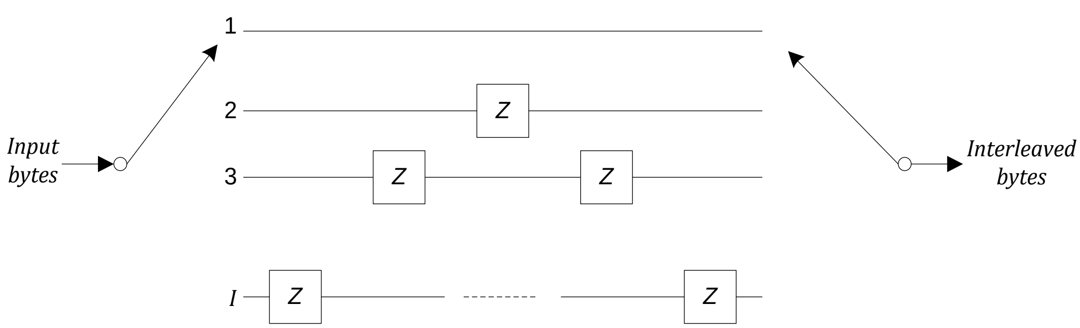

Figure 3.5 Convolutional interleaving structure

Theoretically, Z should be chosen such that [5]

$$Z \geq \frac{E}{\left\lfloor \frac{t-v}{q} \right\rfloor I} = \frac{INP \times B}{\left\lfloor \frac{t-v}{q} \right\rfloor I} \tag{3.7}$$

where *B* is the number of bytes in a DMT symbol, *INP* defines the maximum number of successive correctable corrupted DMT symbols. For example, an impulse of 250μs duration can corrupt two successive DMT symbols. In this case, an *INP* of 2 is needed to correct up to two DMT symbols. $q = n/I$ and v is the number of byte errors in a RS codeword. v is considered to be zero since the system is operating under BER<10^{-22}. $t = \lfloor (n-k)/2 \rfloor$ for ED and $t = (n-k)$ for EED. Since v is approximately considered as zero, when t is doubled in EED, the minimum value of Z can be reduced by half. Hence, the delay caused by interleaving/de-interleaving

$$DELAY = \frac{S \times (D-1)}{q \times f_s} \times \left(1 - \frac{q}{n}\right) = \frac{S \times IZ}{q \times f_s} \times \left(1 - \frac{q}{n}\right) \ (ms) \tag{3.8}$$

can be reduced by half. Here, S is the number of DMT symbols per RS codeword, f_s is the DMT symbol rate of 4 ksymbols/s, and $D = IZ+1$ is the interleaving depth.

3.2 Chapter Summary

In this chapter, we provide an introduction of DSL system, where a general system model is presented. The impact of impulse noise on data transmission is briefly described. To protect DSL system from impulse noise, RS coding and convolutional interleaving are employed. However, the problem of long delay caused by interleaving/de-interleaving arises. To reduce the interleaving delay, EED can be employed instead of ED.

Chapter 4

Squared-Distance Based Erasure Marking Technique for Delay Reduction in DSL Systems Impaired by Impulse Noise[1]

To fully exploit the error correction capacity of EED, it is important to mark erasures exactly. This chapter proposes a squared-distance based erasure marking technique that aims to improve the reliability of erasure flags. Hence, the error correction capacity of the EED can be fully explored and, in turn, the interleaving delay can be reduced.

This chapter is arranged as follows. Section 4.1 provides a literature review on current erasure marking techniques. Section 4.2 proposes an erasure marking technique with three critical thresholds (γ, N_w, N_t). Also presented is the analysis to select the optimal thresholds for the proposed solution. Section 4.3 validates the analysis and provides simulation results to show the delay reduction performance. Finally, Section 4.4 summarizes this chapter.

4.1 Erasure Marking Techniques: Literature Review

As discussed in Chapter 3, EED can be used instead of ED to improve the error correction capacity, and hence to reduce the interleaving delay. However, to perform EED, the additional information indicating whether or not a received byte is in erasure should be passed to the RS-decoder. It is noted that only when accurate erasures are marked, the error correction capacity of EED can be fully explored and correspondingly half interleaving delay can be achieved. To provide accurate erasure flag for RS decoder, several techniques have been proposed to mark erasures. More specifically, the work in

---

[1] Parts of this chapter are presented in [14].

[5] considers a squared-distance based technique, where a received symbol is marked as an erasure if the Euclidean distance between this symbol and the corresponding demodulated one exceeds a distance threshold γ. It is noted that [5] chooses $\gamma = 5\sigma$, where $\sigma^2=\sigma_w^2/2$ is the one-dimensional variance of the background noise [15]. Then, three possibilities are proposed to mark received symbols in a DMT symbol:

i) Only erase the received symbols that are actually marked as erasures according to the squared-distance condition;

ii) Erase the whole DMT symbol (consisting of several modulated symbols) if the number of erasures in this DMT symbol is non-zero;

iii) Erase the whole DMT symbol if the number of erasures in this DMT symbol exceeds a threshold (reference [5] however does not specify this threshold).

The illustrative results in [5] only consider the second possibility. This leads to many falsely marked DMT symbols. Since one DMT symbol contains several RS codewords, all RS codewords in the erased DMT symbol are erased. Subsequently, the number of erasures in these RS codewords exceeds the error correction capacity. Therefore, longer interleaving is required to spread erasures into several DMT symbols to limit the number of erasures in each RS codeword within its error correction capacity. In such a case, interleaving delay in [5] cannot be cut to half of that in ED. In [16], a double-pass algorithm is suggested to mark byte erasures simply by checking the output of the RS decoder. When decoding fails, DMT symbols corresponding to code bytes of the unsuccessfully decoded codeword are marked as erasures. Then, erased DMT symbols are passed through RS decoder again with erasure flag. This double-pass technique does not require any cooperation between the demodulator and decoder. The work in [17] describes an erasure marking technique that uses the information provided by the decoder of an inner code to locate potentially corrupted bytes. However, it needs access to decoder metric and can only be applied to systems using an inner code. Reference [3] presents the analysis of selecting interleaver parameters, summary and comparison of all three techniques in [5], [16] and [17]. As shown in [3], EED with the assistance of these techniques offers a similar interleaving delay reduction of about 20% - 30% compared to ED.

4.2 Proposed Erasure Marking Technique

Our proposal is to mark the suspected code byte as erasure and pass the erasure flag to the RS decoder (in Figure 2.1) to perform EED. In QAM demodulator (part of the DMT demodulator), each received QAM sample R_m is mapped to the nearest QAM symbol $\hat{A}_m$. If the Euclidean distance between them, $|R_m - \hat{A}_m|$, is larger than a selected threshold γ, then, this received sample R_m is marked as an erasure (as shown in Figure 4.1). If the number of marked erasures in N_w exceeds a selected threshold N_t, the *whole* corresponding window is erased. Otherwise, the window is left unmarked as illustrated in Figure 4.2. Demodulated QAM symbols after erasure marking are de-interleaved to be finally decoded by the RS error-and-erasure decoder. Clearly, in the proposed erasure marking technique, three parameters (γ, N_w, N_t) should be properly selected to reap the optimal interleaving delay.

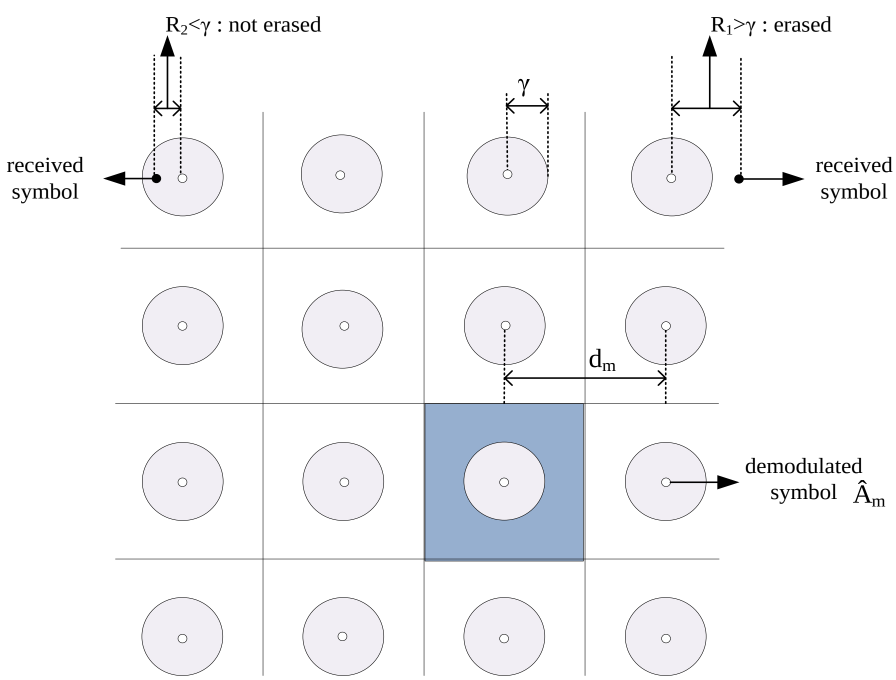

Figure 4.1 Distance threshold γ with erasure marking area

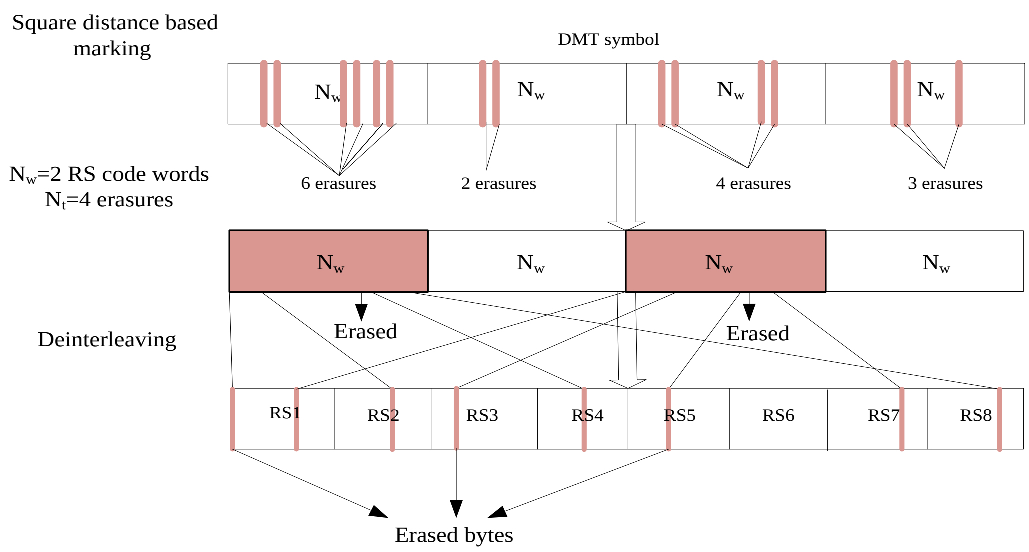

Figure 4.2. Proposed squared-distance based erasure marking technique

4.2.1 Distance Threshold γ

When impulse noise is present, it may move the received sample R_m outside the circle area of the corresponding transmitted symbol A_m in Figure 4.1. In this case, the received sample will be marked as a suspected erasure. Depending on the selected distance threshold γ, there exist cases in which, when IN is present, the received symbol R_m is either still inside the circle area of A_m or inside another circle area (e.g., the impulse power is very strong). In such scenarios, no erasure is marked, and we denote this as missed-detection (i.e., the presence of impulse noise is not detected), namely P_m. Note that in the latter case (i.e., R_m lies inside another circle area), the symbol is erroneously demodulated. In the absence of impulse noise, sometimes the received symbol R_m can be outside the circle area of A_m. As a result, the erasure marking is not correct, namely false-alarm denoted as P_f. Large miss-detection and false alarm probability make the erasure marking less reliable. Hence, both P_m and P_f should be kept as small as possible. It is important to note that the smaller γ, the smaller P_m and the larger P_f, and vice versa. Based on this observation, in considering P_m and P_f of equal importance, we propose to select the distance threshold γ to minimize $P_m + P_f$, representing good trade-off between P_m and P_f.

Let H_0 be the hypothesis that impulse noise is absent, and H_1 be the hypothesis that impulse noise is present. From (3.4) and (3.5), signal models under H_0 and H_1 are:

$$\text{Under } H_0\text{: } R_m = C_m A_m + W_m, \tag{4.1}$$

$$\text{Under } H_1\text{: } R_m = C_m A_m + I_m + W_m. \tag{4.2}$$

Then, the problem of selecting γ is formulated as

$$\gamma_{opt} = \text{argmin}_{\gamma} \{P_m + P_f\}. \tag{4.3}$$

To ease the analysis we solve the optimization in (4.3) under the assumption of the Bernoulli-Gaussian impulse noise model as described in Chapter 2.

<u>Under H_0</u>

The symbol error probability of the square M_m-QAM is [18]

$$\begin{aligned} P_{e,m|H_0} &= 4K_m Q\left(\sqrt{2g_{QAM,m}Y_m}\right) \\ &\quad -4K_m^2 Q^2\left(\sqrt{2g_{QAM,m}Y_m}\right), \end{aligned} \tag{4.4}$$

where $Y_m=|C_m|^2 E\{|A_m|^2\}/\sigma_w^2$, $K_m=1-\frac{1}{\sqrt{M_m}}$, $g_{QAM,m}=3/2/(M_m-1)$, $E\{|A_m|^2\}=(M_m-1)d_m^2/6$ is the average symbol energy, d_m is the minimum distance between two modulated symbols, $Q(x)=\frac{1}{\pi}\int_0^{\frac{\pi}{2}} e^{\left(-\frac{x^2}{2\sin^2\theta}\right)}d\theta$, and $Q^2(x)=\frac{1}{\pi}\int_0^{\frac{\pi}{4}} e^{\left(-\frac{x^2}{2\sin^2\theta}\right)}d\theta$.

The probability that R_m is correctly demodulated is $(1-P_{e,m|H_0})$. This is the probability that the received signal R_m falls in the square decision area containing the demodulated signal $\hat{A}_m$ in Figure 4.1. The probability that the received signal R_m falls within a circle with the radius γ and the center being the demodulated signal $\hat{A}_m$ is

$$\begin{aligned} \Pr\{|R_m - C_m\hat{A}_m| \le \gamma | H_0\} &= \Pr\{|W_m| \le \gamma | H_0\} \\ &= \int_0^{\gamma} \frac{2r}{\sigma_w^2} e^{-\frac{r^2}{\sigma_w^2}} dr = \left(1 - e^{-\frac{\gamma^2}{\sigma_w^2}}\right). \end{aligned} \tag{4.5}$$

From (4.4) and (4.5), we infer P_f (i.e., the probability that the received symbol R_m falls into the circle area in Figure 4.1 under H_0) as

$$P_f = \left(1 - P_{e,m|H_0}\right) - \Pr\left\{\left|R_m - C_m \hat{A}_m\right| \leq \gamma \middle| H_0\right\}. \tag{4.6}$$

It is noted that in the above derivations we do not consider the probability that the received signal R_m falls into another decision area but still outside the circle area, since that under a BER of lower than 10^{-22}, this probability is negligibly small [5].

<u>Under H_1</u>

The symbol error probability of the square M_m-QAM when the DMT symbol is contaminated by both AWGN and IN can be expressed as:

$$\begin{aligned} P_{e,m|G,H_1} = {} & 4K_m Q\left(\sqrt{2g_{QAM,m} Y_{m|G,H_1}}\right) \\ & -4K_m^2 Q^2\left(\sqrt{2g_{QAM,m} Y_{m|G,H_1}}\right), \end{aligned} \tag{4.7}$$

where

$$Y_{m|G,H_1} = \frac{|C_m|^2 E\{|X_m|^2\}}{\sigma_{w,G}^2}, \tag{4.8}$$

$$\sigma_{w,G}^2 = \sigma_w^2 + \sigma_{I|G,H_1}^2 = \sigma_w^2 + \frac{G}{N}\sigma_i^2. \tag{4.9}$$

Variable G is the number of time-domain IN samples in a DMT symbol, and $\sigma_{I|G,H_1}^2$ is the average IN power which can be obtained from (3.5). It is easily seen from Figure 4.1 that the probability that R_m is correctly demodulated is (1- $P_{e,m|G,H_1}$). Similar to (4.5), the probability that the received signal R_m falls within a circle with radius γ and the center being the demodulated signal $\hat{A}_m$ is thus:

$$\begin{aligned} \Pr\left\{\left|R_m - C_m \hat{A}_m\right| \leq \gamma \middle| G, \mathrm{H}_1\right\} &= \Pr\{|W_m| \leq \gamma | G, \mathrm{H}_1\} \\ &= \int_0^{\gamma} \frac{2x}{\sigma_{q|G,H_1}^2} e^{-\frac{x^2}{\sigma_{q|G,H_1}^2}} dx = 1 - e^{-\frac{\gamma^2}{\sigma_{q|G,H_1}^2}}. \end{aligned} \tag{4.10}$$

From (4.7) and (4.10), the conditional probability of good-detection (i.e., the received symbol R_m falls into the blue shadow area in Figure 4.1) when there are G impulse noise samples in one DMT symbol is expressed as

$$P_{g|G} = \left(1 - P_{e,m|G,H_1}\right) - \Pr\left\{\left|R_m - C_m\hat{A}_m\right| \le \gamma \middle| G, \mathrm{H}_1\right\}. \tag{4.11}$$

Then, it is easy to infer the probability of good detection as:

$$P_g = \sum_{G=1}^{N} P_{g|G} \Pr\{G|\mathrm{H}_1\}, \tag{4.12}$$

where $\Pr\{G|\mathrm{H}_1\}$denotes the probability that G impulse noise samples are present in one DMT symbol under H_1. For Bernoulli-Gaussian IN, $\Pr\{G|\mathrm{H}_1\}=\frac{\binom{N}{G}p^G(1-p)^{N-G}}{(1-(1-p)^N)}$.

Since the event of miss-detection is complementary to the event of good-detection, we have:

$$P_m=1-P_g . \tag{4.13}$$

In order to get the solution of (4.3), we take the derivative of $P_m + P_f$ and set it to zero

$$\frac{d\left(P_m+P_f\right)}{d\gamma} = \sum_{G=1}^{N} \frac{\binom{N}{G}p^G(1-p)^{N-G}\left(-\frac{2\gamma}{\sigma_{w,G}^2}e^{-\frac{\gamma^2}{\sigma_{w,G}^2}}\right)}{(1-(1-p)^N)} + \frac{2\gamma}{\sigma_w^2}e^{-\frac{\gamma^2}{\sigma_w^2}} = 0. \tag{4.14}$$

We can numerically obtain the solution of (4.14), γ_{opt}. It is clear that the value of γ_{opt} is related to the variance and occurrence probability of impulse noise (i.e., $\sigma_i^2$and p).

4.2.2 Window Size N_w and Selecting Threshold N_t

The erasure marking technique in [5] chooses the window size N_w to be equal to one DMT symbol and the selecting threshold N_t equal to one modulated symbol. This does not offer a significant reduction in interleaving delay. In this subsection, we discuss the selection of N_t to achieve the minimum interleaving delay. Given a window size N_w, a small threshold N_t can cause too many windows to be erased, possibly the number of erasures exceeding the error correction capability of EED. For successful decoding, these erasures must be distributed over many codewords by increasing the interleaving depth. On the other hand, a large threshold N_t will cause almost no erasure, resulting in the ED mode, and thus, requiring a long interleaving. To explain the effects of N_t on interleaving delay, we investigate the distribution of number of erasures after de-interleaving.

The system parameters are listed in Table 4.1. We consider a frequency-flat fading channel with 256-QAM. Although this channel model is not realistic in practical DSL systems, it nevertheless provides an insight into the effects of N_t on the interleaving delay and intuitively explains the observed results. The interleaving parameter is selected as $I = n$ bytes (hence, $q = n/I$). In the simulation, the value of Z is increased until the BER after decoding gets to sufficiently small [5]. Then, the minimum value of Z is applied to (3.8) to compute the minimum interleaving delay, which is 8 ms for ED, and expected to be 4 ms for EED. Consider a Bernoulli-Gaussian IN model with a high PSD of -90dBm/Hz, and parameter p selected to be relatively low such that for most cases only one time-domain impulse sample occurs during one DMT symbol. Let N_{era} be the number of marked erasures in each RS codeword after de-interleaving.

Table 4.1 System parameters

Parameter	**Value**
PSD of transmitted signal	-60dBm/Hz
PSD of AWGN	-140dBm/Hz
Impulse noise model	Bernoulli-Gaussian impulse noise
PSD of impulse noise	-90dBm/Hz
Probability of impulse noise occurrence	$p = 4 \times 10^{-6}$
Number of tones	4096
Frequency spacing	4. 3125kHz
DMT symbol rate	4 ksymbol/s
Band plan	Profile 12a [19]
SNR margin	6dB
Target BER	10^{-7}
RS code parameters	(128, 112) bytes

Interleaving parameters	(I, Z) bytes

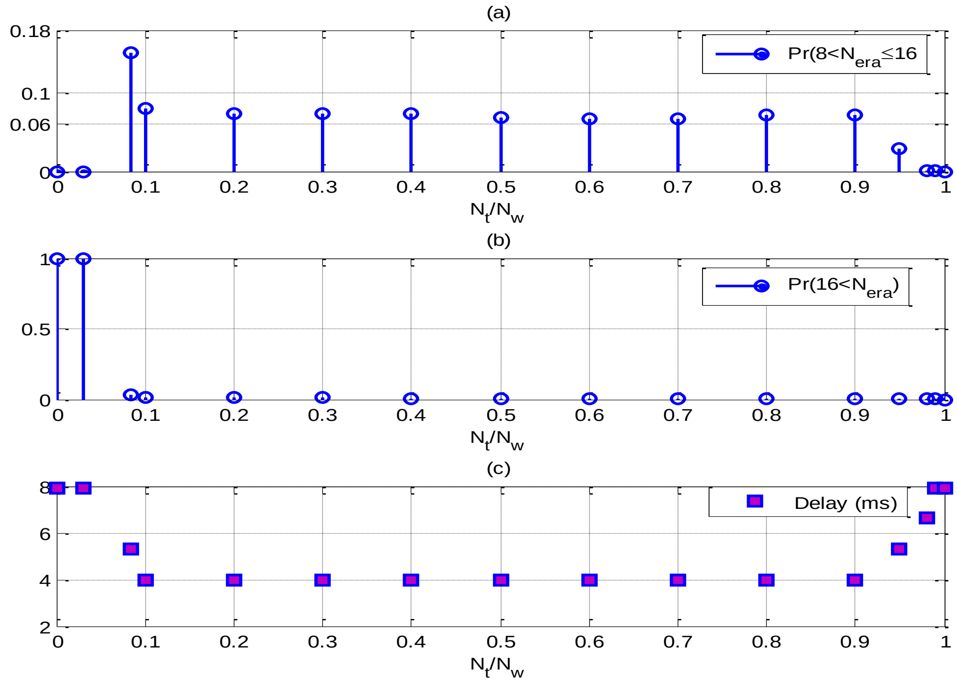

Figure 4.3 Pr{8 <N_{era} ≤ 16}, Pr{16 <N_{era} }, and Corresponding interleaving delay

Here N_w is equal to one DMT symbol, and it is clear that for 0.1≤N_t/N_w≤0.9, Pr{8 <N_{era} ≤ 16} is larger than 0.06. When N_t/N_w= 0.95, this probability drops to around 0.03, which means that some erasures are missed-detected due to the increase of N_t/N_w. As N_t/N_w increases to 0.98, Pr{8 <N_{era} ≤ 16} further drops to almost zero, implying that more erasures are missed-detected and the decoder is almost driven to work in the ED mode. However, by examining the number of actual byte errors in each RS codeword, namely N_e, after de-interleaving while setting the interleaving delay to 4 ms (i.e., the expected minimum interleaving delay for EED), Pr{8<N_e≤16} is more than 0.05% as shown in Table 4.2. Therefore, the ED cannot correct all the errors in these codewords with 4ms delay, since N_e in some RS codewords exceeds the error correction capacity (i.e., t = 8) of the ED. So for N_t/N_w≥ 0.95, the BER after the decoder is high that longer interleaving will be required to spread the errors further since only by increasing delay to 8ms, Pr{8<N_e≤16 } will drop to zero and the number of errors in each RS code is within the error correction capacity of ED.

Table 4.2 Distribution of number of erasures in one RS codeword after de-interleaving

Interval	$0 \leq N_e \leq 8$	$8 < N_e \leq 16$	$16 < N_e$
Probability with 4 ms delay	99.947%	0.053%	0
Probability with 8 ms delay	100%	0	0

For $0 \leq N_t/N_w \leq 1/12$, a longer delay is expected. To explain this, let investigate Pr{$16 < N_{era}$}, where 16 is the error correction capacity of EED. From Figure 4.3 (b), it is clear that for N_t/N_w = 0, 1/32 or 1/12, Pr{$16 < N_{era}$} is nonzero, implying that the number of erasures in some RS codewords exceeds the error correction capacity of EED due to many falsely marked erasures. For these cases, the BER after decoding is high and longer interleaving is expected.

4.3 Simulation Results and Discussions

In this section, we first validate the analysis for selecting the optimal distance threshold γ. Then, we provide the interleaving delay reduction performance for the proposed erasure marking technique.

4.3.1 Validation of Analytical Results

For consistency and simplicity, all the simulations are carried out with parameters presented in Table 4.1. We consider a frequency-flat fading channel response. Since the modulation level for each tone is identical, the minimum distance d between two modulated symbols is the same. For Bernoulli-Gaussian IN model, we choose a relatively small p so that at most two IN samples will occur during one DMT symbol. Under these settings, (4.12) can be approximated as:

$$P_g \approx \frac{\binom{N}{1} p(1-p)^{N-1} P_{g|1}}{1-(1-p)^N} + \frac{\binom{N}{2} p2(1-p)^{N-2} P_{g|2}}{1-(1-p)^N}, \tag{4.18}$$

Subsequently, the miss-detection probability becomes:

$$P_m \approx 1 - \frac{\binom{N}{1} p(1-p)^{N-1} P_{g|1}}{1-(1-p)^N} - \frac{\binom{N}{2} p^2(1-p)^{N-2} P_{g|2}}{1-(1-p)^N}. \tag{4.19}$$

As a result, (4. 14) can be simplified as:

$$\frac{\binom{N}{1}p(1-p)^{N-1}\left(-\frac{2\gamma}{\sigma^2_{q|1,\mathrm{H}_1}}e^{-\frac{\gamma^2}{\sigma^2_{q|1,\mathrm{H}_1}}}\right)}{1-(1-p)^N} + \frac{\binom{N}{2}p^2(1-p)^{N-2}\left(-\frac{2\gamma}{\sigma^2_{q|2,\mathrm{H}_1}}e^{-\frac{\gamma^2}{\sigma^2_{q|2,\mathrm{H}_1}}}\right)}{1-(1-p)^N} + \frac{4\gamma}{\sigma^2_w}e^{-\frac{\gamma^2}{\sigma^2_w}} = 0. \tag{4.20}$$

In the simulations, exhaustive search is used to find γ that minimizes $P_m + P_f$. More specifically, P_m is calculated by counting the number of demodulated symbols in a DMT symbol that are not erased when IN hits that DMT symbol, and P_f is computed by counting the number of demodulated symbols in a DMT symbol that are erased when no IN happens in that DMT symbol.

In Figure 4.4, we plot P_m, P_f, and $P_m + P_f$ versus $\gamma/(d/2)$. Clearly, the simulation and analytical results for both P_m and P_f are well matched, and the minimum value of P_m+P_f is obtained at $\gamma/(d/2)=0.3$. It is noted that $\gamma/(d/2)=0$ implies that each received modulated symbol is marked as erasure and $\gamma/(d/2)=1$ means that almost no erasure is marked[2]. It is clear that, as γ increases, P_m increases (i.e., the increase of the radius leads to the increase of circle area in Figure 4.1, implying fewer marked erasures) while P_f decreases (i.e., the circle area increases as γ increases, and correspondingly the shaded area in Figure 4.1 shrinks, resulting in fewer detected erasures).

[2] There may still be some erasures as the symbol may fall into the corner area in Figure 4.1. However, this chance is typically low that we can ignore it, since the circle area almost cover the square area when $\gamma/(d/2) = 1$.

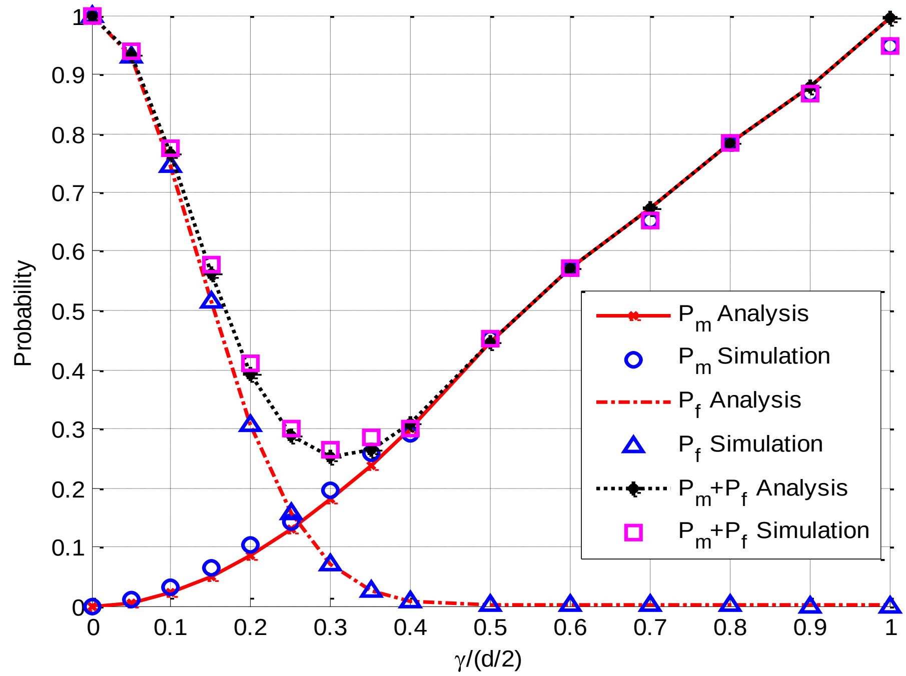

Figure 4.4 P_m**,** P_f **and** P_m**+**P_f

4.3.2 Interleaving Delay Reduction

1) Simulation Parameters:

Simulations carried out in this subsection using parameters and values listed in Table 4.3. We investigate six cases with respect to different IN models, channel conditions, γ values, and erasure marking methods as listed in Table 4.4.

Table 4.3 Common system parameters

Parameter	**Value**
PSD of transmitted signal	-60dBm/Hz
PSD of AWGN	-140dBm/Hz
Number of tones	4096
Frequency spacing	4. 3125kHz
DMT symbol rate	4 ksymbol/s
Band plan	Profile 12a [19]

SNR margin	6dB
Target BER	10^{-7}
RS code parameters	(n, k) bytes
Interleaving parameters	(I, Z) bytes

Table 4.4 Specifications for 6 cases

Case 1	Bernoulli-Gaussian IN, frequency-selective fading and flat-fading channel, γ_{opt} from analysis, mark the individual received symbol only based on γ
Case 2	Bernoulli-Gaussian IN, flat-fading channel with fixed QAM 256, γ_{opt} from analysis, N_w is equal to one DMT symbol
Case 3	Bernoulli-Gaussian IN, frequency-selective fading channel, γ_{opt} from analysis, N_w from one RS codeword to one DMT symbol
Case 4	Bernoulli-Gaussian IN, frequency-selective fading channel, γ_{opt} from simulation, N_w is equal to one DMT symbol
Case 5	REIN, frequency-selective fading channel, γ_{opt} from simulation, mark the individual received symbol only based on γ
Case 6	REIN, frequency-selective fading channel, γ_{opt} from simulation, N_w from one RS codeword to one DMT symbol

Case 1 considers both the flat-fading channel and frequency-selective fading channel obtained through the measurement on the 500m 25-pair 26-AWG cable bundle [20]. We only mark erasure when the distance between the received and the demodulated symbol is larger than γ.Case 2 is with the same 256-QAM on all tones but with the proposed erasure marking technique. Case 3 investigates the proposed erasure marking technique over the frequency-selective fading channel. For Case 4, we set the same $\gamma_{opt}/(d_m/2)$ for all the subcarriers. This value of $\gamma_{opt}/(d_m/2)$ is obtained by exhaustive search, in which $\gamma/(d_m/2)$ is changed from 0 to 1 with a step size of 0.1, and the optimal $\gamma/(d_m/2)$ that yields the smallest P_m+P_f is selected. Case 5 is the same simulation scenario as Case 1 but with REIN and a frequency-selective fading channel. Case 6 is carried out with the proposed technique while 250 μs REIN is injected.

2) Simulation results

a) Case 1: Table 4.5 shows the delay reduction performance for Case 1 with (128, 112) RS code. It is clear that there is no delay reduction for flat-fading channel, whereas the delay reduction achieved in frequency-selective fading channel is 16.7%. From this case, reducing the delay by 50% as illustrated in theory is impossible if erasures are marked only based on the squared-distance condition, since there are some bytes falsely marked or miss-detected.

Table 4.5 Interleaving delay for one-step erasure marking based on γ

Channel	Delay for ED (ms)	Delay for EED (ms)	Delay reduction percentage
Flat-fading	8	8	0
Frequency-selective fading	8	6.67	16.67%

b) Case 2: Results on the delay performance are shown in Figure 4.5. Here, we still consider the (128, 112) RS code. For simple demonstration, we simulate with the window size N_w equal to one DMT symbol.

Figure 4.5 shows that there exists an optimal range of N_t that yields a minimum delay of 4 ms, which is half of the delay in ED (i.e., 8 ms), in agreement with our previous discussions in Section 4.2.2. For a fair comparison with [5], we also obtained simulation results for the same configuration of Case 2 with γ=5σ, and N_t=1 modulated symbol (shown by the "brown diamond" in Fig. 6). It is observed that the selection of γ=5σ, and N_t=1 (or $N_t/N_w=3.3\times10^{-4}<0.1$) is not optimal, and interleaving delay reduction is not significant. The results in [5] show the interleaving delay reduction of EED over ED of about 20% to 30% for IN which corrupts up to two DMT symbols (i.e., the impulse duration is less than or equal to 250μs). For the same scenario, our proposed erasure marking scheme can guarantee an interleaving delay reduction of 50% for a wide range of N_t.

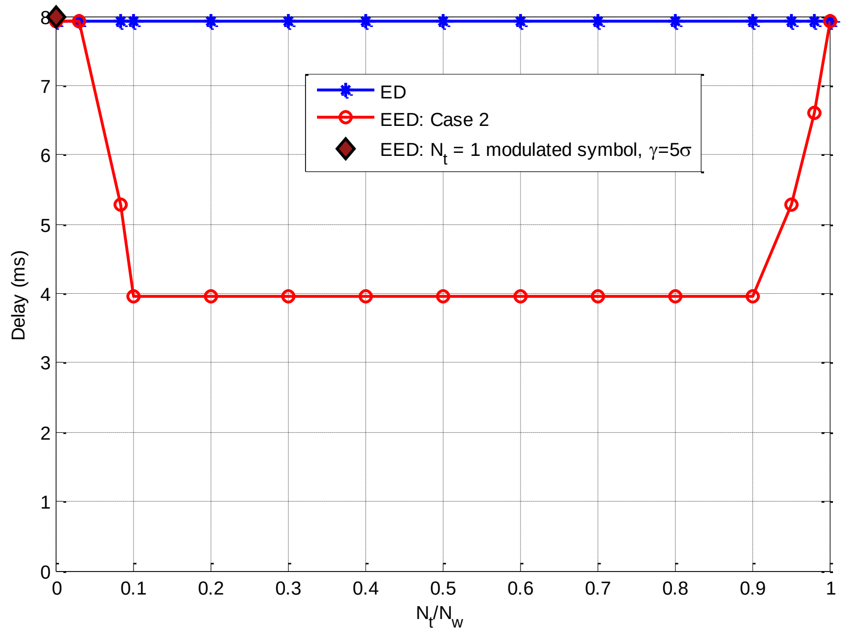

Figure 4.5 Interleaving delay: Case 2

c) Case 3: We select different N_w from one RS codeword length to one DMT symbol. From Figure 4.6, it is clear that similar to Case 2, when $0.28 \leq N_t/N_w \leq 0.8$, a minimum delay of 4 ms is achieved. Additionally, the optimal range of the threshold N_t grows wider as N_w increases. Since larger N_w offers a wider range of optimal N_t (implying in a more flexible and safer choice of N_t), it is more appropriate and practical to choose N_w as one DMT symbol.

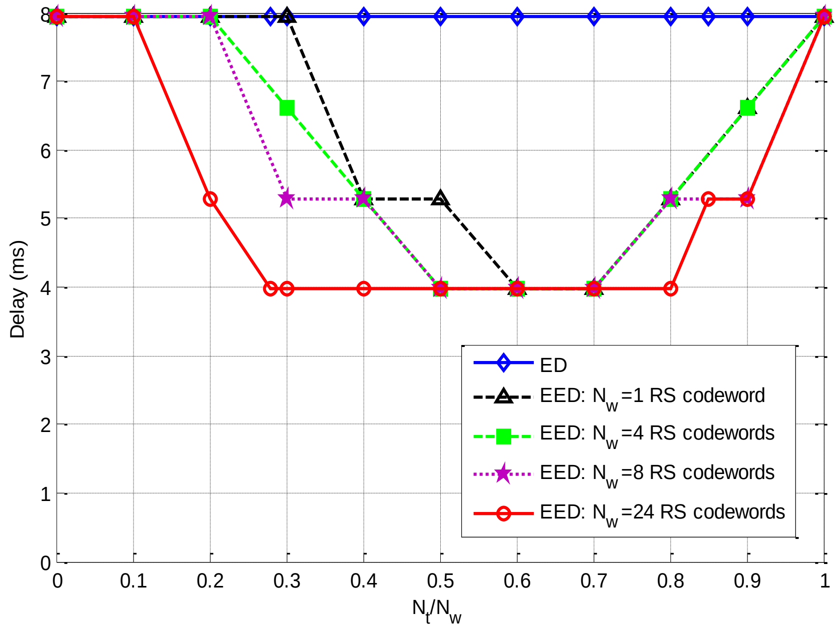

Figure 4.6 Interleaving delay: Case 3

d) Case 4: Different from Case 2, $\gamma_{\text{opt}}/(d_m/2)$ is obtained from simulation and fixed for all subcarriers. From Figure 4.7, it is clear that the 4ms delay can be achievedfor $0.25 \leq N_t/N_w \leq 0.55$. However, this range is much narrower than what are previously observed in Cases 2 and 3.

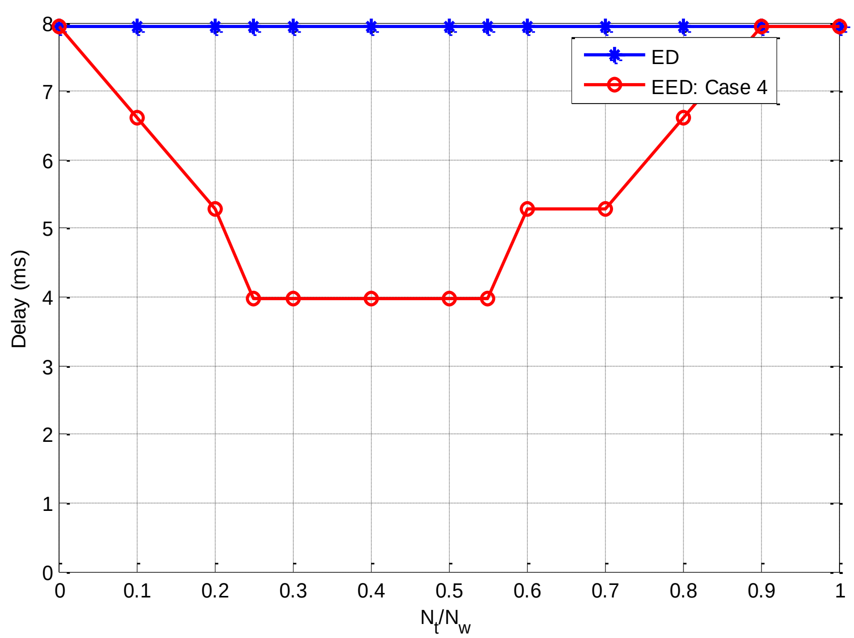

Figure 4.7 Interleaving delay: Case 4

e) Case 5: Table 4.6 shows the interleaving delay for both ED and EED which mark erasures only based on the squared-distance condition. In this table, IN1, IN2, and IN3 denote three different kinds of REIN with different durations of 250µs, 500µs, and 750µs, respectively. The delay reduction ratio is defined as ($DELAY_{ED}$-$DELAY_{EED}$)/$DELAY_{ED}$, where $DELAY_{ED}$ and $DELAY_{EED}$ denote the interleaving delay for ED and EED, respectively. It can be seen that for the same impulse duration, a stronger RS code implies a smaller delay reduction (e.g., for the impulse duration of 250µs, the delay reduction percentage is 11.1% and 20% for the strong RS code (n=64, k=48) and the weaker RS code (n=128, k=112), respectively). For the same RS code, the delay reduction is improved with larger impulse duration (e.g., for the RS code (n=64, k=48) the delay reduction percentage is 11.1%, 14.3%, and 16.7% for the impulse duration of 250µs, 500µs, and 750µs, respectively).

Results in Table 4.6 demonstrate that the delay reduction with only squared-distance condition is not optimal and the maximum delay reduction is approximately 25%.

Table 4.6 Interleaving delay reductions for case 5

		(n, k)	(I, Z)	Delay (ms)	Delay reduction percentage
ED	IN1 (250µs)	(64, 48)	(64,9)	3.9375	0
		(128,112)	(128,5)	7.9375	0
	IN2 (500µs)	(64, 48)	(64,14)	6.125	0
		(80,64)	(80,12)	7.9	0
	IN3 (750µs)	(64, 48)	(64,18)	7.875	0
EED	IN1 (250µs)	(64, 48)	(64,8)	3.5	11.1%
		(128,112)	(128,4)	6.35	20%
	IN2 (500µs)	(64, 48)	(64,12)	5.25	14.3%
		(80, 64)	(80,9)	5.925	25%
	IN3 (750µs)	(64, 48)	(64,15)	6.5625	16.7%

f) Case 6: Simulations in this case are carried out with the (n=128, k=112) RS code and the REIN of 250µs duration. The results shown in Figure 4.8 are similar to those in Figure 4.6.

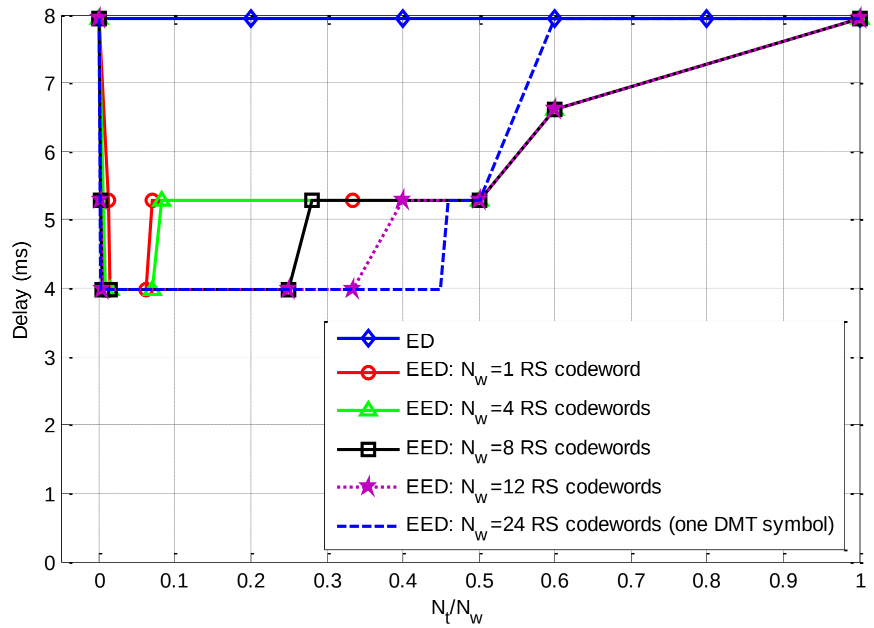

Figure 4.8 Interleaving delay: Case 6

To sum up, marking erasures only based on γ is not reliable, while the proposed technique proves to be efficient in erasure marking with a delay reduction of half as compared to ED. To further consider the proposed erasure marking technique, it is appropriate to choose N_w as one DMT symbol as this is more practical in real DSL implementations. More importantly, this guarantees a more flexible and safer choice of N_t that can achieve optimal delays.

4.4 Chapter Summary

In this chapter, we have shown that the interleaving delay of DSL systems corrupted by IN is significantly reduced by properly marking erroneous code bytes before EED. Erasure marking is obtained by comparing the distances between the received and the demodulated symbols with threshold γ. Then, we further check if erase the whole N_w using threshold N_t. Analysis on selecting the optimal γ is developed and validated. Simulation results with various channel conditions and IN models show that the proposed technique provides an interleaving delay reduction by 50% compared to ED. For the optimal delay reduction, choosing N_w to be equal to one DMT symbol is the most practical and efficient way. Moreover, the proposed technique can be easily incorporated in practical DSL systems since only modifications in the demodulator are needed and EED has already been an option in current DSL systems [19].

Chapter 5

Video Performance over DSL in presence of IN with Efficient Erasure Marking Technique

In this chapter, we evaluate the erasure marking based delay reduction technique in video transmission. This chapter is organized as follows. Section 5.1 introduces a general system model of video transmission. Delay in video transmission is emphasized. The impact of IN on video transmission is examined in Section 5.2. The criterion to measure video quality is also stated. Simulation results will be provided to demonstrate the efficiency of the proposed erasure marking technique. Section 5.3 concludes the chapter.

5.1 Video Transmission over Impulsive DSL Systems

Video over DSL systems is vulnerable to impulse noise corruption. Without any protection, the video packet-loss due to the effects of IN can be very serious. Although RS coding and interleaving/de-interleaving are employed to protect video against IN distortion, long latency, which is not desirable in some video applications, such as interactive Television and online video games [6], is introduced.

Figure 5.1 presents a general system model for video transmission over DSL system in presence of IN.

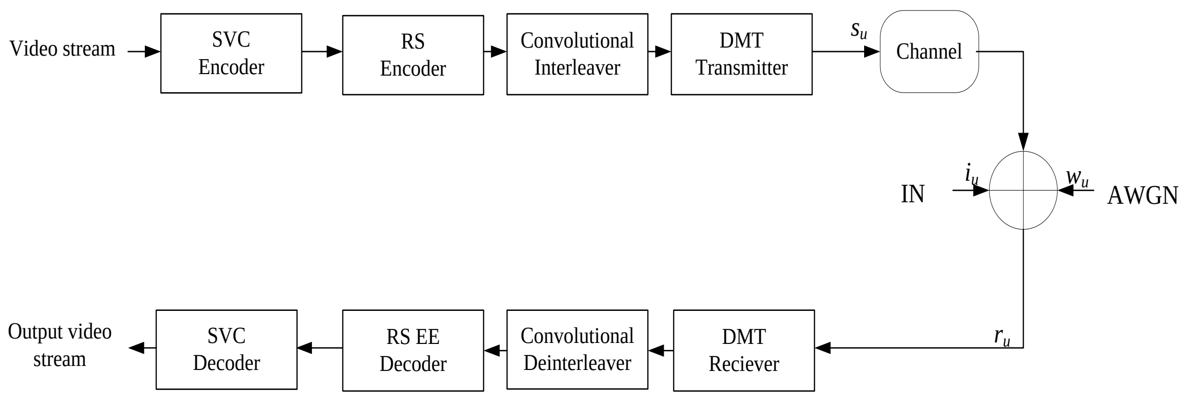

Figure 5.1 Video transmission over DSL system affected by IN

This model is the same as the system model in Chapter 3, except that a scalable video coding (SVC) encoder is used to convert video stream to binary stream and the output binary data is remerged and converted back to video stream by the SVC decoder. By comparing the input and output video stream, PSNR is obtained to determine the quality of the output video, which is calculated as follows:

$$PSNR_{linear} = \sum_{i} \frac{255^2}{MSE_i} \tag{5.1}$$

$$PSNR_{log} = 10log_{10}(PSNR_{linear}) \tag{5.2}$$

where 255 is the maximum pixel value with 8 bits per sample pixel and the mean square error MSE_i is given by:

$$MSE_i = \frac{1}{hw} \sum_{m=0}^{h_v} \sum_{j=0}^{w_v} (S_o\,[\mathrm{m,j}] - S_r\,[m,j])^2 \tag{5.3}$$

Here, $S_r[m,j]$ denotes the sample value obtained from the output video file, $S_o[m,j]$ is the sample value from the original video file, and h and w are the height and width of the video, respectively. Therefore, it is clear that the higher the video distortion (i.e., higher MSE), the lower the PSNR.

5.2 Video Transmission Performance:

The PSNR as well as BER performance versus various delays with ED is shown in Figure 5.2. The simulation scenario is the same as Figure 4.8 except that compressed video file is used as the input data. It is noted beforehand that PNSR ≈ 45 dB indicates good video quality [21]. From Figure 5.2, when the delay is short (i.e., Delay≤5.33 ms), PSNR is low that almost all the frames are lost and the corresponding BER is high (i.e., around 10^{-2}). As the delay is increased to 6.67ms, PSNR is improved by about 18dB and BER drops to around 10^{-4}. By increasing delay to 8 ms, PSNR increases to 45 dB and the BER is less than 10^{-7}.

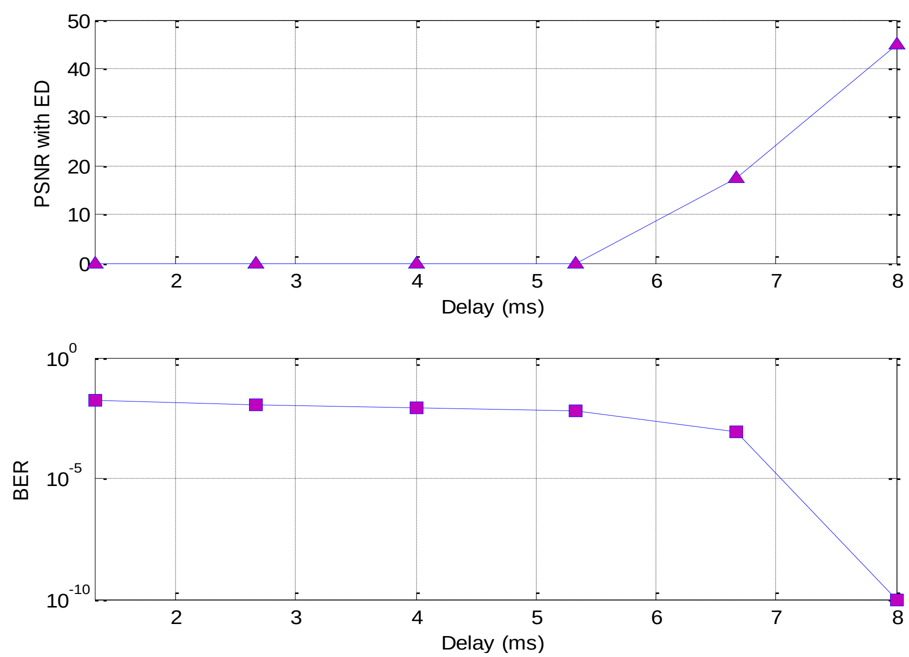

Figure 5.2 PSNR and BER for ED versus different delays

Simulation with the same scenario but employing EED and proposed erasure marking technique is depicted in Figure 5.3. To illustrate the problem, N_w is equal to 1 DMT symbol. The distance threshold γ is obtained as stated in Case 5 in Chapter 4. It shows PSNR performance with 4ms delay and the delay performance versus different N_t/N_w. It is clear that for $1/12 \leq N_t/N_w \leq 0.45$, the PSNR is around 45dB, showing good output video quality is maintained with 4 ms delay. For $N_t/N_w \leq 1/14$, due to the fact that too many erasures are marked that the number of erasures in RS codeword exceeds the error correcting capacity of EED, longer delay is required. For$0.6 \leq N_t/N_w$, the marked erasures are too few that it is almost in the ED mode and 8 ms delay is required.

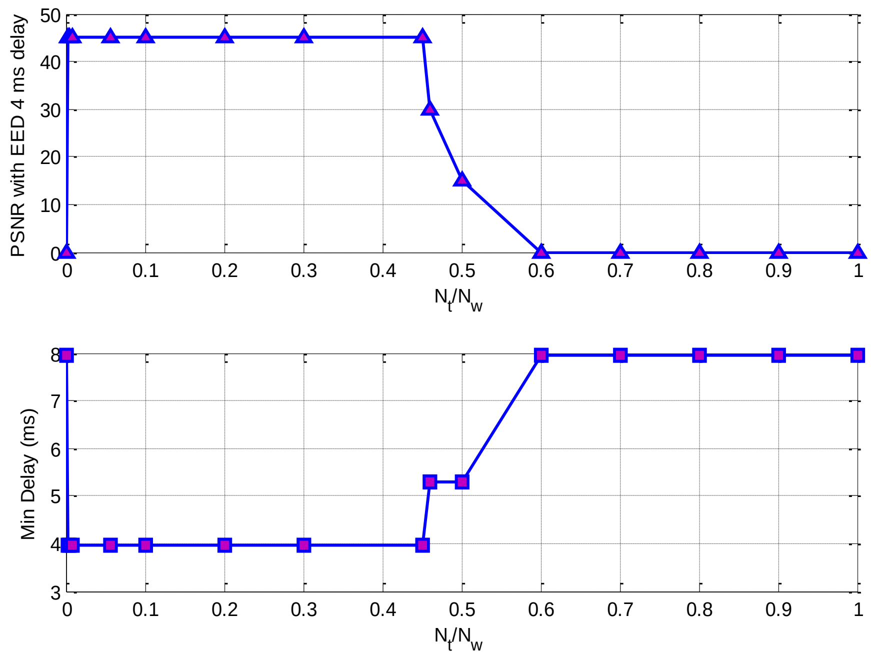

Figure 5.3 PSNR and minimum delay for EED

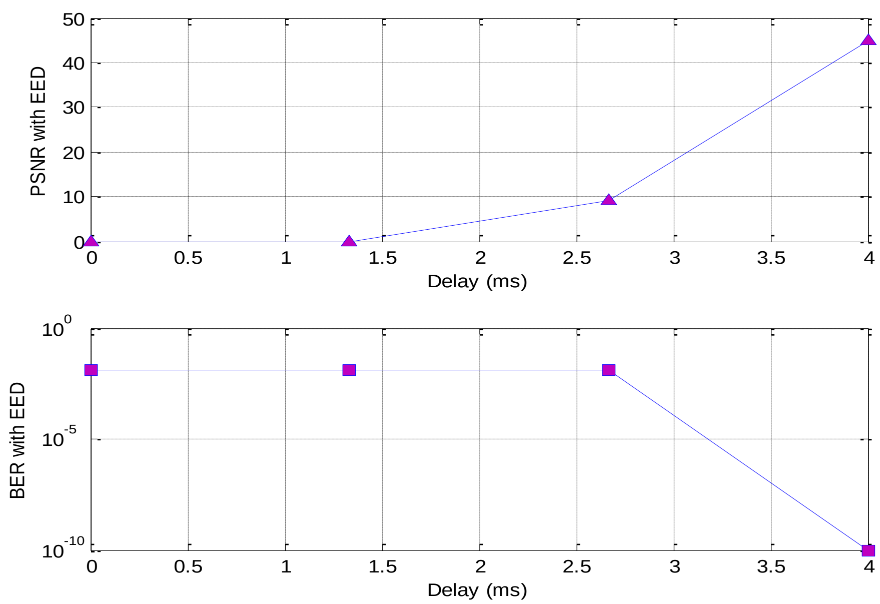

Figure 5.4PSNR and BER for EED versus different delays

Figure 5.4 compares the PSNR and corresponding BER performance versus different delay when EED is enabled. In this case, N_w is equal to one DMT symbol and N_t/N_w=0.3, where 4 ms delay is achieved. It is seen from the figure that as delay increases, PSNR increases, while BER decreases. This is consistent with the results in Figure 5.2.

For a more intuitive demonstration, video captures of the same frame from different video files are shown. Figure 5.5 is taken from the original video file to be used as a reference. To show that for ED case, insufficient delay cannot protect the video from IN distortion, we capture the same frame from the output video file with 6.67ms delay as shown in Figure 5.6. Great distortion can be seen, since a minimum delay of 8 ms is required for ED.

Figure 5.5 Original video frame

Figure 5.6 Captured Video frame: ED with insufficient delay (6.67ms delay)

However, when the proposed erasure marking is employed, and the distance threshold and selecting threshold N_t are properly chosen, good video quality can be obtained with 4ms delay, as shown in Figure 5.7.

Figure 5.7 Captured Video frame: EED with 4 ms delay

5.3 Chapter Summary

In this chapter, we first introduce the system model of video transmission over DSL system impaired by IN and PSNR as one way to measure video quality. Simulations with both ED and the proposed erasure marking technique have been carried out and compared. Results show the good BER performance indicating high PSNR, and the proposed erasure marking technique is efficient in reducing delay by half while maintaining good video quality.

Chapter 6

Conclusions

This chapter provides the conclusion of the work done in this thesis and discusses some potential subjects possibly interesting for further work.

6.1 Conclusions

In this thesis, we proposed an efficient erasure marking technique that mark accurate erasures, and hence fully explore the error correction capacity of EED. Correspondingly, the delay caused by interleaving and de-interleaving is reduced by half as compared to ED.

For impulse noise modeling, the distribution of inter-arrival time and amplitude can be modeled by an exponential and a Gaussian distribution, respectively. Moreover, we conclude that IN generated by hair dryer follows a Bernoulli-Gaussian process.

Regarding the proposed erasure marking technique, an analytical method to select the optimal distance threshold γ is proposed and validated. The value of threshold N_t has a great effect on delay reduction performance. Simulation results with different channel conditions, IN models and γ values have shown that the proposed erasure marking technique provides reliable erasure information with properly selected γ and N_t. Correspondingly, the interleaving delay with EED is reduced by half as compared to ED.

In addition, video transmissions with the proposed erasure marking technique embedded show that delay caused by interleaving and de-interleaving can be reduced by half as compared to ED, while the video quality is maintained.

6.2 Suggested Future Work

Although we successfully demonstrated the effectiveness of the proposed erasure marking technique, there are still some following aspects that may be interesting to be studied further.

The analysis of selecting optimal γ presented in Chapter 4 is based on the Bernoulli-Gaussian impulse noise model. An extension of this analysis to consider different IN models such as REIN can be an interesting subject for further studies. Also, other criteria to select the optimal γ could be proposed and compared.

In addition, we only provide simulation results for the effects of threshold N_t. An analytical method to select the optimal value of this parameter could be developed.

Furthermore, when the proposed technique is tested with the video file, PSNR is issued as a measure of the video quality. One can go further by investigating the video quality using other performance metrics, such as Perceptual Evaluation of Video Quality (PEVQ), Structural Similarity (SSIM) and Czenakowski Distance (CZD).

References

[1] N. H. Nedev, "Analysis of the impact of impulse noise in digital subscriber line systems," *Ph.D. dissertation*, University of Edinburgh, 2003.

[2] J.M. Cioffi, "A multicarrier primer," *Tutorial*, Stanford University, November 1991.

[3] D. Toumpakaris, J.M. Cioffi, and D. Gardan, "Reduced-delay protection of DSL systems against nonstationary disturbances," *IEEE Transactions on Communications*, vol. 52, pp. 1927-1938, November 2004.

[4] TR-176 1.00 "ADSL2Plus Configuration Guidelines for IPTV," *Technical Report*, Broadband Forum, September 2008.

[5] D. Toumpakaris, J.M. Cioffi, and D. Gardan, "A square distance-based byte-erasure method for reduced-delay protection of DSL systems from non-stationary interference," in *Proc. IEEE Globecom'03*, vol. 4, pp. 2114-2119, Dec. 2003.

[6] ITU-T News Log, "IPTV standardization on track say industry experts," 2006.

[7] M. Tlich, H. Chaouche, A. Zeddam and P. Pagani, "Novel approach for PLC impulsive noise modeling," in *Proc. IEEE International Symposium on Power Line Communications and Its Applications*, Dresden, pp. 20-25, April 2009.

[8] M. Ghosh, "Analysis of effect of impulse noise on multicarrier and single carrier QAM system," *IEEE Transactions on Communications*, vol. 44, pp. 145-147, February. 1996.

[9] C. W. Helstrom, *Probability and Stochastic Processes for Engineers*, New York, Macmillan Publishing Company, 1984.

[10] TR-114 "VDSL2 Performance Test Plan," *Technical Report*, Broadband Forum, November 2009.

[11] W. Henkel, T. Kessler, and H. Y. Chung, "Coded 64-CAP ADSL in an impulse-noise environment-modeling of impulse noise and first simulation results," *IEEE*

Journal on Selected Areas in Communications, vol. 13, pp. 1611 – 1621, December 1995.

[12] S. Wicker, *Error Control Systems for Digital Communication and Storage*, Englewood Cliffs, New Jersey, Prentice-Hall, 1995.

[13] G. C. Clark, Jr. and J. B. Cain, *Error-correction coding for digital communications*, New York, Plenum Press, 1981.

[14] Y. Zhao, K. Ho-Van, T. Le-Ngoc, "Efficient erasure marking technique for interleaving delay reduction in DSL systems impaired by impulse noise," *IEEE International Conference on Communications*, Ottawa, Ontario, 2012.

[15] T.N. Zogakis, P.S. Chow, J. T. Aslanis, and J.M. Cioffi, "Impulse noise mitigation strategies for multicarrier modulation," in *Proc. IEEE International Conference on Communications*, vol. 2, pp. 23–26, May 1993.

[16] D. Toumpakaris, W. Yu, J.M. Cioffi, D. Gardan, and M. Ouzzif, "A simple byte-erasure method for improved impulse immunity in DSL," in *Proc. IEEE International Conference on Communications*, vol. 4, pp. 2426-2430, May 2003.

[17] D. Toumpakaris, W. Yu, J. M. Cioffi, D. Gardan, and M. Ouzzif, "A byte-erasure method for improved impulse immunity in DSL systems using soft information from an inner code," in *Proc. IEEE International Conference on Communications*, vol. 4, pp. 2431-2435, May, 2003.

[18] K.Cho, and D.Yoon, "On the general BER expression of one and two-dimensional amplitude modulations," *IEEE Transactions on Communications*, vol. 50, no. 7, pp. 1074-1080, 2002.

[19] ITU-T Rec. G.993.2 Std., *Very High Speed Digital Subscriber Line transceivers* 2 (VDSL2), February 2006.

[20] R. Morawski, K. Ho-Van, D. Zhang, and Y. Zhao, "xDSL channel response and quiet line noise: Measurement and Results," *Technical Report*, McGill University, May 2010.

[21] D. Padmanabhan, "Report- SVC test suite and results of testing," *Technical Report,* McGill University, January 2010.